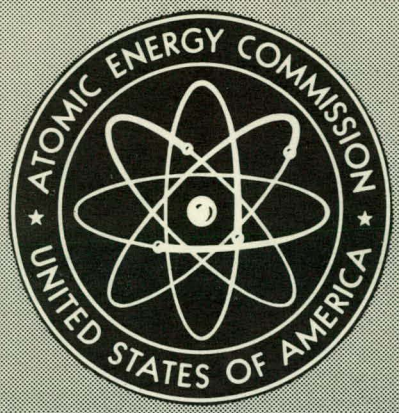

GA-3409

DIFFERENTIAL NEUTRON THERMALIZATION

Annual Summary Report, October 1, 1961 through September 30, 1962

By
W. L. Whittemore

November 28, 1962

General Atomic Division
General Dynamics Corporation
San Diego, California

UNITED STATES ATOMIC ENERGY COMMISSION • DIVISION OF TECHNICAL INFORMATION

DISCLAIMER

LEGAL NOTICE

This report has been reproduced directly from the best available copy.

Printed in USA. Price $1.50. Available from the Office of Technical Services, Department of Commerce, Washington 25, D. C.

USAEC Division of Technical Information Extension, Oak Ridge, Tennessee

PAGES i to iv

WERE INTENTIONALLY

LEFT BLANK

FIGURES (Cont.)

FIGURES (Cont.)

FIGURES (Cont.)

TABLES

I. INTRODUCTION

The experimental and theoretical work carried out during this contract reporting period continues the fundamental studies of the interaction mechanisms by which neutrons exchange energy with hydrogen atoms. Above ~1 ev these interactions may be regarded as collisions of neutrons with free hydrogen atoms; however, at lower energies they must be regarded in terms of excitation of molecular (liquid or crystal) thermal motions determined by binding forces. A problem of neutron thermalization is therefore concerned with the distribution of energy levels and the probability of excitation by neutron collision. In particular, differential neutron thermalization is concerned with specific neutron interactions with these various energy levels. In earlier phases of this contract, the interest was directed toward very-low-temperature moderators for two quite complimentary reasons. On the one hand, in low temperature moderators the binding effects are more apparent and easily studied. On the other hand, an understanding of the cold moderator can serve to optimize the source of high intensity cold neutrons for the present experimental program as well as for research at other reactor projects. As this contract has progressed, the interest has shifted to the specific details of the scattering kernel $\sigma(E_o, E, \theta, T)$ for several moderator substances.

During the first four months of this contract period, a large mechanical, rotating, neutron beam chopper of the Fermi type was designed, constructed and placed in operation. During the subsequent months, the experimental arrangement was improved and utilized to collect data on differential neutron scattering from several hydrogenous materials. Presently (several weeks prior to the end of the present contract period) much experimental data is being produced and is being analyzed. A final report on results for a given moderator is not possible at this time. Consequently, the present report must be considered to be a status report. However, several aspects of cold moderators as they affect the operation of the experimental arrangement have been developed and will be reported in detail here.

To carry out experiments in the areas of interest just discussed, neutrons from a pulsed electron linear accelerator were utilized. The pulsed beam has been previously used as a source of neutrons for neutron spectra and cross-section measurements preliminary to the major measurements in the scattering kernal. The techniques were outlined in the previous Annual Summary Report[1]. Additional, rather special arrangements have to be made to use the pulsed electron beam in conjunction

with the rotating neutron chopper as a velocity selector. Details of the various experimental arrangements, including the use of liquid hydrogen as a source of cold neutrons, will be given in Section II.

At this point, it may be useful to point out the several advantages of the accelerator source of neutrons in observations made on inelastic neutron scattering. The use of a pulsed neutron beam from the linear accelerator with a rotating mechanical chopper to provide a velocity selector gives a significantly different approach to the experimental arrangement in comparison with the usual velocity selector at a reactor. In the first place, it is important to note that, in addition to the linear accelerator, only one rotating mechanical chopper is required. At a reactor it is usual to employ four phased, rotating choppers. In comparing a nuclear reactor on the one hand, and an electron linear accelerator on the other, the additional equipment required to provide a satisfactory velocity selector is much less for the linear accelerator. An additional advantage is that a variable speed nonsynchronous motor is satisfactory for powering the one chopper required. This permits easy changes of speed as the conditions of the experiment change. One of the four choppers usually employed at a reactor in a multiple chopper array is eliminated by using the pulse characteristics of the linear accelerator itself. Two additional choppers used at a reactor to eliminate fast neutron background are not needed at a linear accelerator because of the absence of fast neutrons at detection times significant for most of the experiments.

II. EXPERIMENTAL TECHNIQUES

The method for utilizing an electron linear accelerator to perform neutron spectra measurements and neutron total-cross-section measurements is quite well known by now and was thoroughly discussed in the previous Annual Summary Report[1]; however, the details of the arrangement used currently to perform inelastic neutron-scattering measurements are sufficiently new to warrant the detailed treatment given below.

The physical layout in the experimental hall is much the same as for previous measurements. Figure 1 shows the floor plan of the experimental area of the high-current electron linear accelerator, including the position used for the inelastic scattering measurements. Figure 2 shows the relationship between the various components of the present velocity selector used to select neutrons of various energies from ~0.005 ev up to above 0.20 ev. The various components of the velocity selector will be discussed in order, starting with the electron neutron converter.

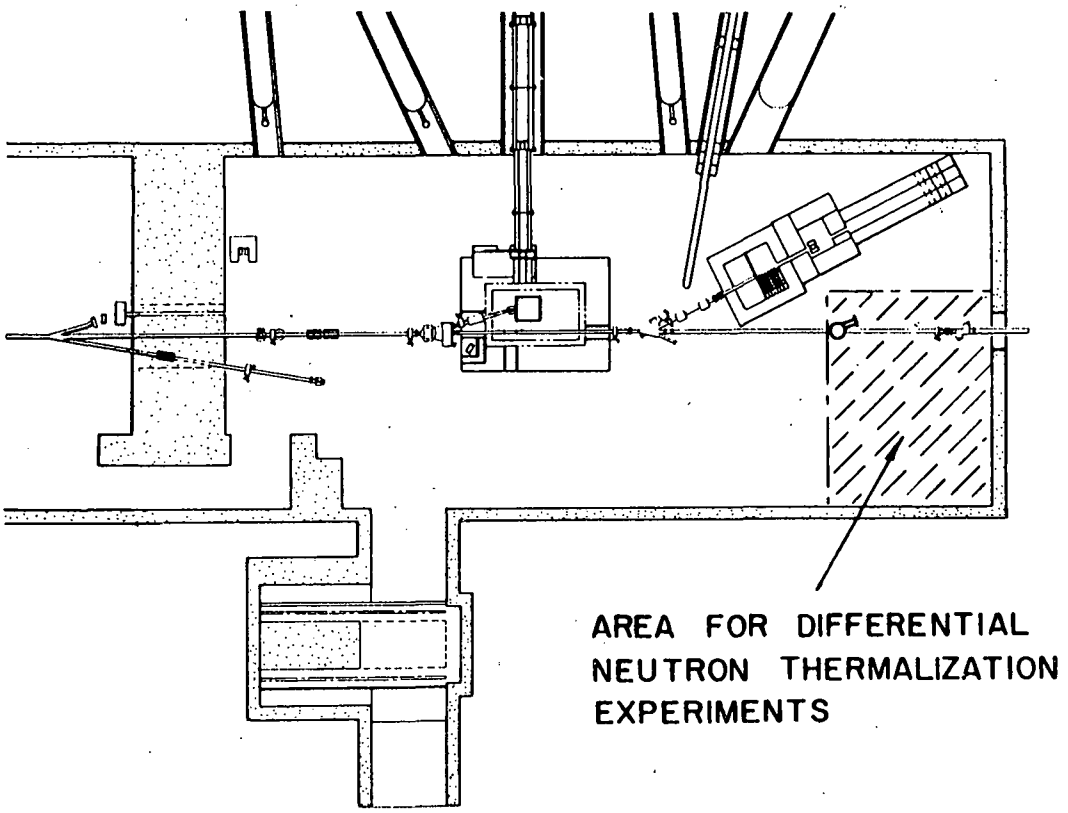

Fig. 1.--Floor plan of the experimental area at the high current electron linear accelerator showing the location of the neutron velocity selector

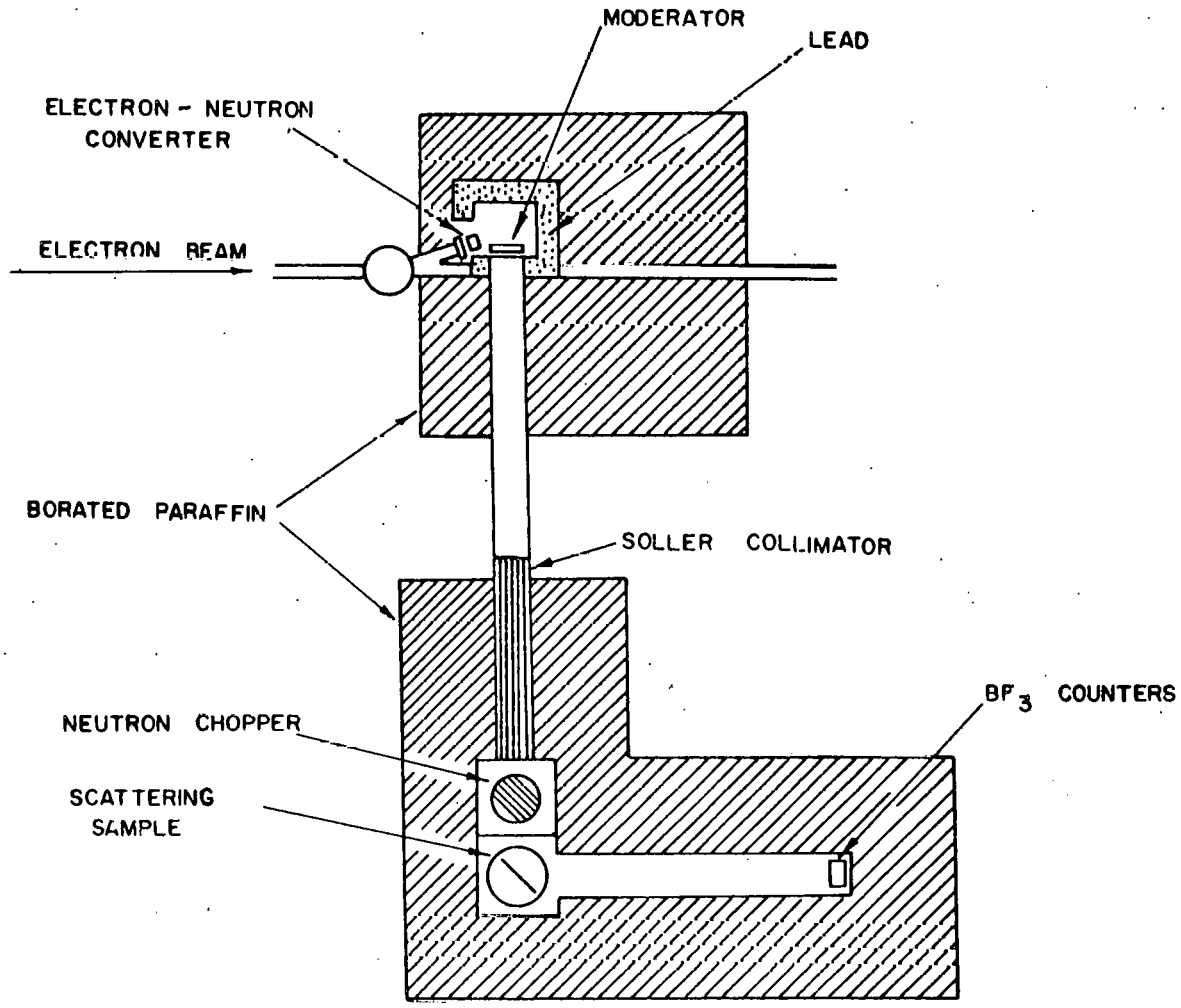

Fig. 2.--Schematic drawing of experimental arrangement of the neutron velocity selector

2.1 NEUTRON SOURCE

The electron beam, which reaches an instantaneous peak of about 0.6 amps, passes out of the beam tube through a thin, water-cooled, aluminum window. The window consists of two thin, parallel, aluminum windows with a thin sheet (~1/8 in.) of water flowing between them at the rate of about 6 gal/min. The dispersion of the well-focused beam by the water layer is insignificant since the electron target is large and is nearby.

2.1.1 Electron-Neutron Converter

The source of neutrons for the thin slab of moderator material is a water-cooled Fansteel target shown in Fig. 3. Fansteel is a high density (17 gm/cc) alloy of 89 percent tungsten, 7 percent nickel and 4 percent copper. This target has been observed in operation to be a considerably more effective source of fast neutrons than the previously used lead target. This is as expected from the larger photo-neutron cross section in tungsten. Uranium 238 has a still larger photo neutron cross section but introduces further complications due to the activation of the target.

2.1.2 Fast Neutron Reflector

The moderator in its low temperature environment is placed close to the Fansteel target inside a lead cave which also houses the electron target. In an effort to maximize the number of thermal neutrons, the maximum solid angle subtended by the moderator at the target is desired. Because the emission of fast neutrons from the target is very roughly isotropic, considerable assistance is obtained from the "fast"-neutron lead reflector which functions to increase the quantity of fast neutrons arriving at the moderator.

Gold foil activations were made to find the preferred location in the cave for the moderator, taking into account the finite size of the moderator and its cooling bath. As expected, the highest intensity of slow neutrons is obtained by moving the moderator as close as possible to the source. However, these measurements have verified that the intensity drops by a factor of less than two if the moderator is moved more than a foot away. Advantage of this distance is taken to construct an insulated, low-temperature, cooling bath. Similar considerations are valid when liquid hydrogen is used as the cold moderator, since the cryostat with its vacuum jacket requires substantial room.

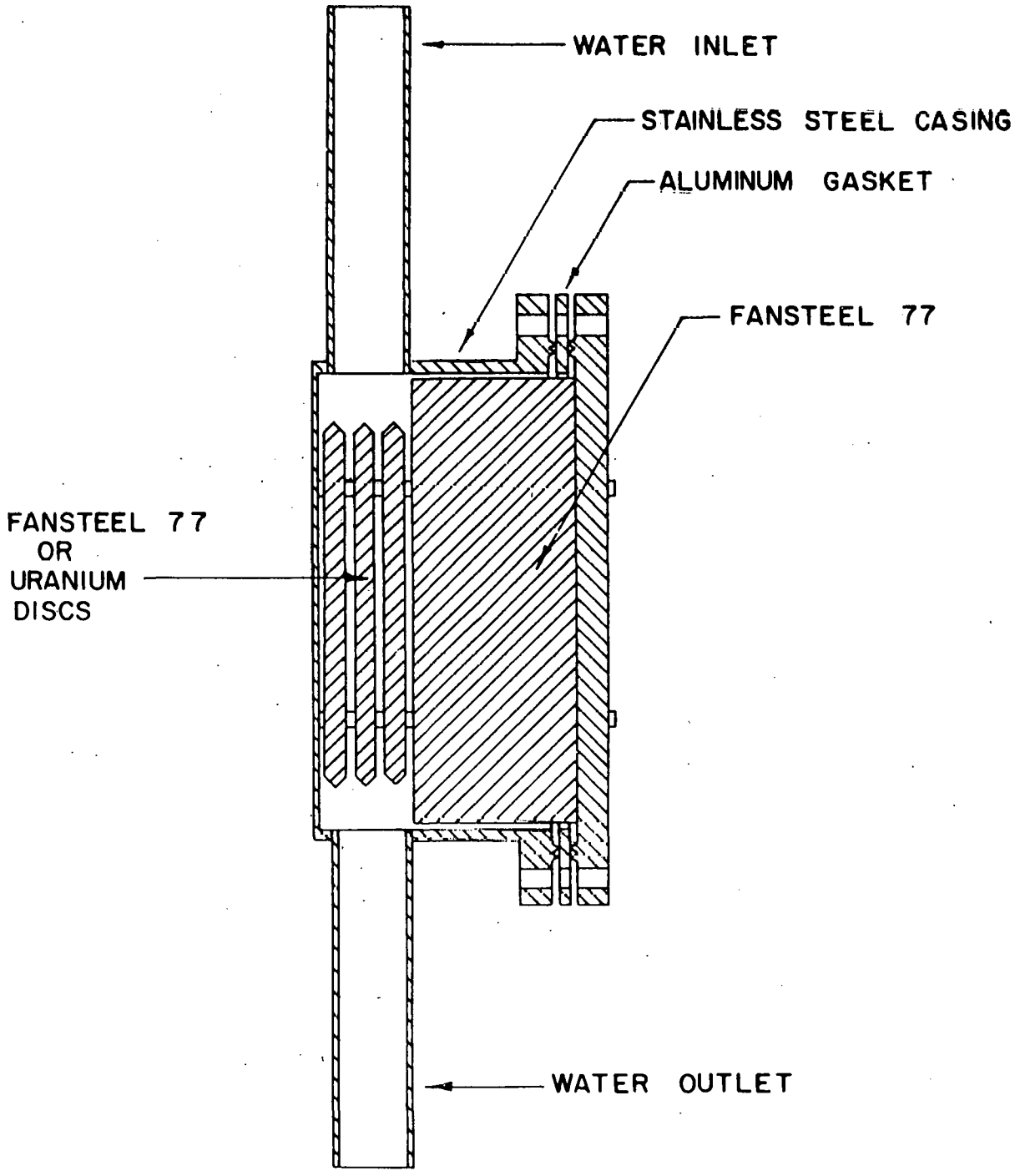

Fig. 3.--Cross section of the electron-neutron converter

2.1.3 Neutron Moderator

For the experiments to be described here, the thermal neutron source is either a slab of paraffin or an appropriate quantity of liquid para-hydrogen. The following three important considerations govern the selection of a particular neutron moderator: (1) radiation damage, (2) thermal neutron intensity, and, (3) time resolution.

During the last several years we have had occasion to use, as cold neutron moderator, slabs of H_2O and CH_2 and liquid H_2 and CH_4. Recently we have found CH_2 to be a reasonable source if it is used in the form of paraffin. Polyehtylene having a similar chemical structure is not suitable for this operation since it explosively erupts after heavy neutron and gamma irradiation. When liquid para-hydrogen is used as the moderator there is some possibility that the hydrogen is dissociated under a strong irradiation, although it is believed that the major result of irradiation is simply evaporation of the hydrogen due to radiative heating of the container.

The beam intensity of thermal neutrons produced depends critically upon the exact geometrical arrangements of the moderator and source. Measurements reported previously[1] have related to a considerably different geometry. It was shown that water, liquid CH_4 and polyethylene were superior to liquid hydrogen for neutron energies exceeding 0.010 ev. For lower neutron energies, liquid para-hydrogen is superior. The use of liquid ortho-hydrogen and the various other solid moderators, such as cold CH_4 and CH_2, are strongly dependent upon the use of a reentrant hole for maximum neutron intensity. While the intensity from para-hydrogen was observed to be less by as much as a factor of two than for the just mentioned substances, for neutron energies less than 0.015 ev it was NOT dependent upon geometrical considerations. Consequently, for the lower energy regions, liquid hydrogen is a good source and is relatively independent of geometrical details. For energies substantially higher than 0.015 ev, other hydrogeneous materials provide considerably greater fluxes of thermal neutrons but are dependent on the geometrical arrangement for the optimum flux.

The time resolution is affected directly by the length of the neutron emission time. For a velocity selector using a pulsed moderator as the first element and a rotating chopper as the second element of the system, the neutron emission time and the source-to-chopper distance are the main determining factors for the time (and hence energy) resolution. Table 1 shows quantitatively the manner in which the energy resolution $\Delta E/E$ depends on these two factors. The data in this Table neglect the effect of the finite chopper-open time.

Table 1

A TABULATION OF COMPUTED VALUES OF $\Delta E/E = 2\Delta T/T$ FOR A NUMBER OF TYPICAL CASES

E (ev)	μsec/meter	$\left[\frac{\Delta E}{E}\right]_1$*	$\left[\frac{\Delta E}{E}\right]_2$	$\left[\frac{\Delta E}{E}\right]_3$	$\left[\frac{\Delta E}{E}\right]_1$	$\left[\frac{\Delta E}{E}\right]_2$	$\left[\frac{\Delta E}{E}\right]_3$
		Source width (half height) (100 μsec)			Source width (half height) (50 μsec)		
.001	2280	.088	.044	.029	.044	.022	.015
.005	1025	.195	.10	.065	.100	.05	.032
.010	720	.278	.14	.092	.139	.07	.046
.025	456	.42	.22	.143	.22	.11	.073
.050	322	.622	.311	.207	.31	.15	.103
.100	228	.878	.44	.29	.44	.22	.15
.150	187		.535	.35		.25	.17
.200	162		.60	.41		.30	.20

*The subscript indicates the source-chopper distance in meters

2.1.4 Neutron Emission Time for Thin Slab Geometry

The time resolution for the incident beam is a stronger consideration than the absolute intensity in many of the measurements to be described. Since the thin slab moderator is the first element of the velocity selector, the shortness of the neutron emission time from this moderator is of prime consideration. The ultimate time resolution for this velocity selector is governed mainly by the so called neutron "die-away" time in the moderator. Consequently, geometrical conditions and types of moderator must be chosen in such a way as to make this pulse as small as possible. This consideration applies equally well when using the linear

accelerator as a source of neutrons for cross section measurements. For those measurements, however, one can use a long flight path to overcome this limitation since the detected beam is longer by several orders of magnitude. Several of the basic ideas have been outlined previously.[1] Additional details of importance to the present arrangement are described here.

The sequence for producing a short burst of "thermal" neutrons with the electron linear accelerator is as follows: A very short burst of "fast" neutrons of approximately 5 μsec duration is produced in the Fansteel target. The moderation of these neutrons proceeds immediately and in about 1 μsec after the fast neutrons are produced, they have moderated to an energy of about 1 ev.[2] The final energy distribution of the neutrons and its time dependence is completely dependent upon the nature and size of the moderator and on its temperature.

Consider for the moment that an infinitely large moderator is supplied with a point source of "fast" neutrons at its center. After the neutrons have reached an energy of about 1 ev (in ~ 1 μsec), they continue making collisions with the lattice until they reach thermal equilibrium with the moderator. This time is of the order of 25 to 50 μsec depending upon the moderator. The neutron population then decreases with time as $e^{-t/\tau}$, where τ, the "die-away" time, is dependent upon the leakage, and hence the size and shape as well as constitution, of the moderator. For large moderators of hydrogeneous material, this time can be several hundred μsec. Since the "die-away" is a consequence of the neutron leakage from the surface of the moderator, it can be reduced if the moderator dimensions are small. If the geometry is that of a slab with very small dimensions in one direction, the "die-away" time can be reduced considerably. However, it has been demonstrated in a number of experiments that the minimum neutron emission time for a slab moderator is usually of the order of 50 to 100 μsec.

In the preceding discussion, a very large moderator was considered. With moderator dimensions drastically reduced, experimental neutron spectrum measurements indicate that the neutrons are still nearly in thermal equilibrium with the moderator. Even for rather small moderators the equilibrium distributions of neutrons is still emitted over a rather long time. By cooling the moderator so that the average equilibrium energy is far below that of the desired neutron energy the observed neutron emission time decreases significantly, presumably because the neutrons are then part of the slowing-down spectrum and are not the equilibrium distribution. Experience

has shown that the energy down to which the slowing down spectrum can thus be extended is approximately 5 times the thermal Maxwellian peak. This means that a sharp pulse can be produced for neutrons having energy greater than 0.0085 ev (5 x .0017 ev) in liquid hydrogen. In polyethylene at 77°K, short emission times exist for neutrons with energies down to about 0.035 ev, since the thermal peak appears at about 0.007 ev.

For best resolution and thermal neutron intensity, from either a liquid para-hydrogen or polyethylene moderator at 77°K, one has the following considerations. For incident energy, $E_o < 0.009$ ev, the use of para-hydrogen is better though not optimum. The neutron pulse is rather long (characterizing the "die-away" time of the moderator) but the intensity of neutrons from para-hydrogen is larger than from CH_2, especially for $E_o < 0.005$ ev. For $0.009 < E_o < 0.035$ ev, the best moderator for thermal neutrons is clearly para-hydrogen as far as time resolution is concerned, although there will be some sacrifice in intensity. For $E_o > 0.035$ and from the point of view of intensity, the better choice is CH_2, though both moderators produce short pulses. For $E_o > 0.15$ ev, CH_2 at room temperature is a reasonable choice.

2.1.5 Measurement of Neutron Emission Time

Since the pulse shape from a thermal neutron source, particularly its width at half its maximum height, is important in the determination of the time resolution, an experimental program has been underway for a long time to determine precisely this time characteristic of the moderated thermal neutron beam. Two rather different techniques have been used for the investigation: (1) a crystal diffraction technique and, (2) a beam chopper technique.

Crystal Diffraction - For some of the investigations of pulse shapes produced by a thin slab of moderator, a crystal of magnetic Fe_3O_4 was used to determine the neutron emission time from the moderator. From the basic Bragg relation, $n\lambda = 2d \sin\theta$, one sees that $d(n\lambda)/n\lambda = \cot\theta \, d\theta$ and that $d(n\lambda)/n\lambda$ can be made arbitrarily small by decreasing $d\theta$, the angular aperture subtended at the crystal by the source. If $d(n\lambda)/n\lambda$ is made small compared to the expected value of $\Delta T/T$, then the neutrons selected by the crystal will arrive at the detector according to their emission time from the moderator. Since the time of flight permits one to detect simultaneously several orders, $n\lambda$, then

one setting of θ gives a number of energies spaced according to n^2. Typically, it is possible to measure the emission time simultaneously for 0.025, 0.100, and 0.225 ev or simultaneously for 0.010, 0.040, 0.090 and 0.160 ev, depending on the value of θ chosen for the diffracting crystal.

Typical experimental results are shown in Figs. 4 and 5 where the neutron emission time was determined for a slab geometry using polyethylene CH_2 with 1-cm and 5-cm thicknesses. The first order energies were selected to be about 0.009 and 0.039 ev, both of which are less than twice the thermal energy. For the 5-cm slab (see Fig. 4) one sees clear evidence at 0.039 ev for the "die-away" time, which is most evident in the wing of the pulse at long flight times. At higher energies, the pulse is approximately triangular and has a full width of $\sim 7 \times 16$ μsec whereas, at 0.04 ev, the pulse is $\sim 31 \times 16$ μsec including a long "die-away" time. Note that these times are full width at the base, whereas time-of-flight analysis customarily uses full width at half the maximum height as the criterion. The results for a 1-cm slab show that, even for 0.039 ev, the long "die-away" time is greatly reduced so that the full width of the pulse is 7×16 μsec compared to $\sim 31 \times 16$ μsec.

Figures 6 and 7 show greater detail for the pulse shape (neutron emission time) from a 2-inch slab of CH_2 at 77°K and a 6-inch layer of liquid para-hydrogen. In Fig. 6, the difference in emission time from CH_2 for neutron energies of 0.014 ev (about $2.2 \times kT_{77}$) and 0.054 ev (about $8.5 \times kT_{77}$) is striking. The results for para-hydrogen, shown in Fig. 7, show less of an extended "tail" on the emission curve for a neutron energy of 0.014 ev ($8 \times kT_{20}$) but exhibit a rather large width at half maximum (108 μsec) compared to that for neutrons having 0.054 ev ($31 \times kT_{20}$). This width of 108 μsec is dependent on the thickness of para-hydrogen and can be less for a 2- or 4-inch slab. The substantial dependence of the neutron emission time on thickness, moderator and temperature is readily apparent.

As a parenthetical remark, it may be worth noting that the crystal diffraction technique has applicability for the measurement of neutron "die-away" times performed for reactor physics problems, expecially when the "die-away" time for one specified energy is of interest.

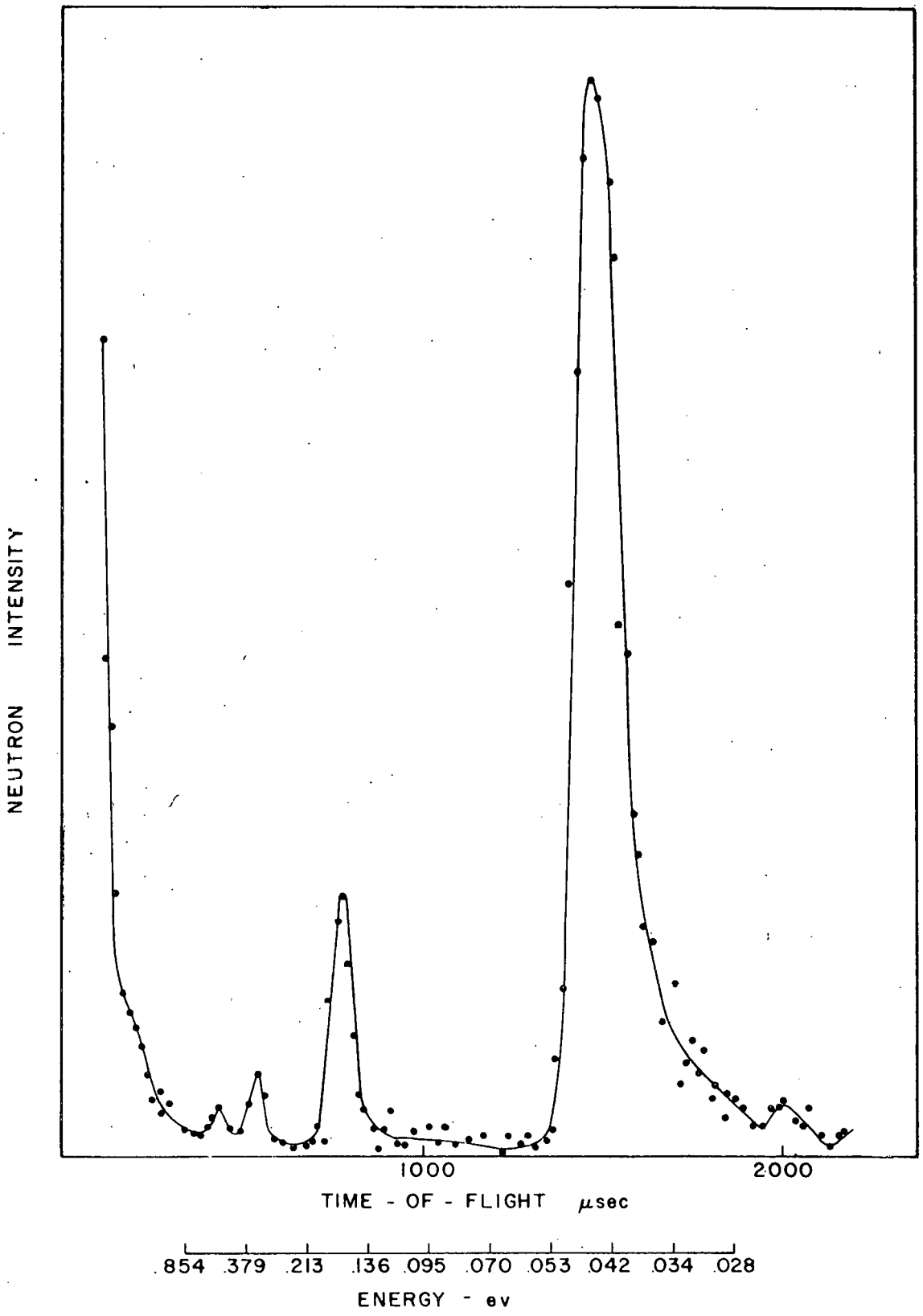

Fig. 4.--Emission times of neutrons selected by (111) planes in magnetite and produced by a 5-cm slab of polyethylene at 300°K

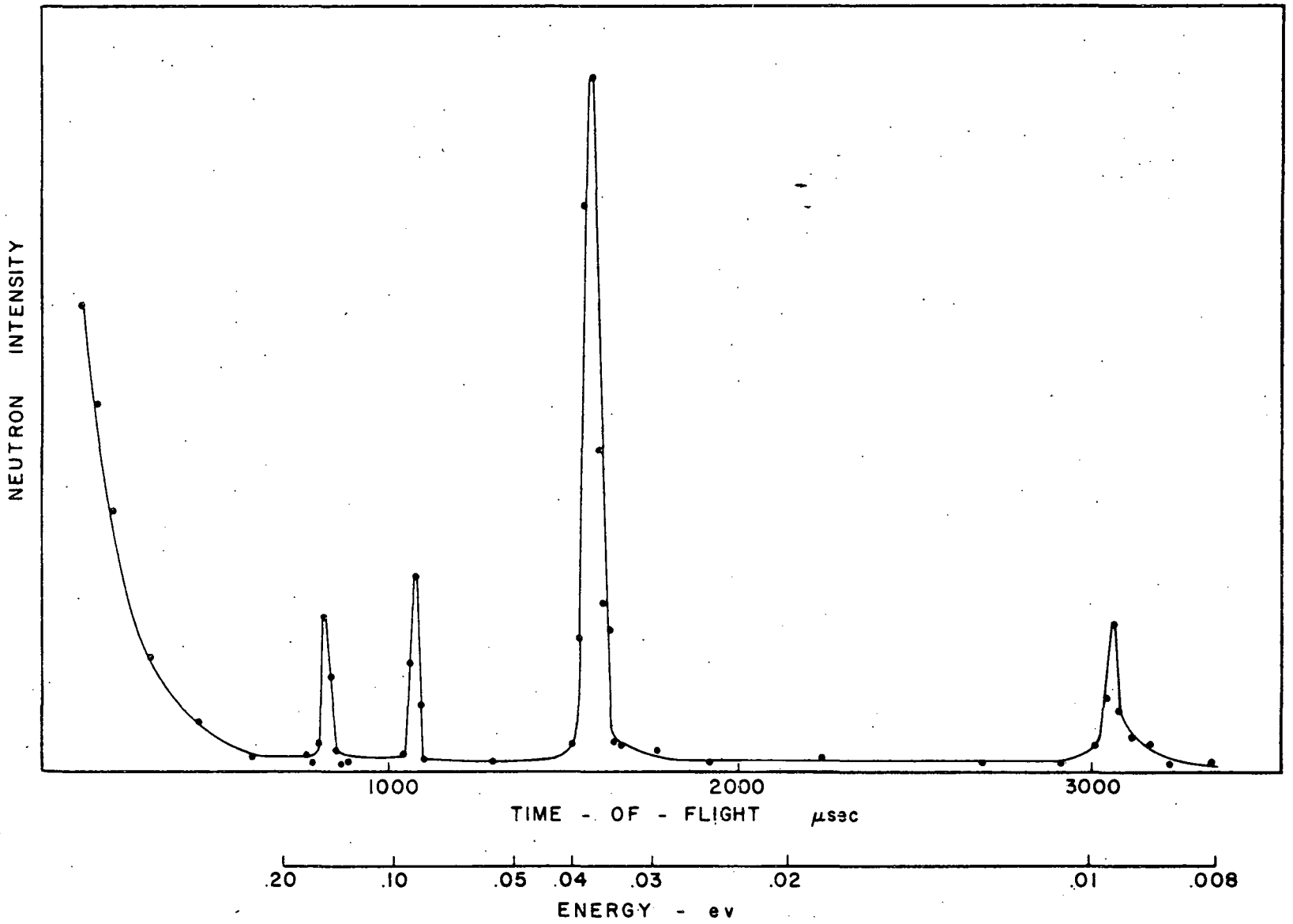

Fig. 5.--Emission times of neutrons from a 1-cm slab of polyethylene at 300°K selected by the (111) planes of Fe_3O_4

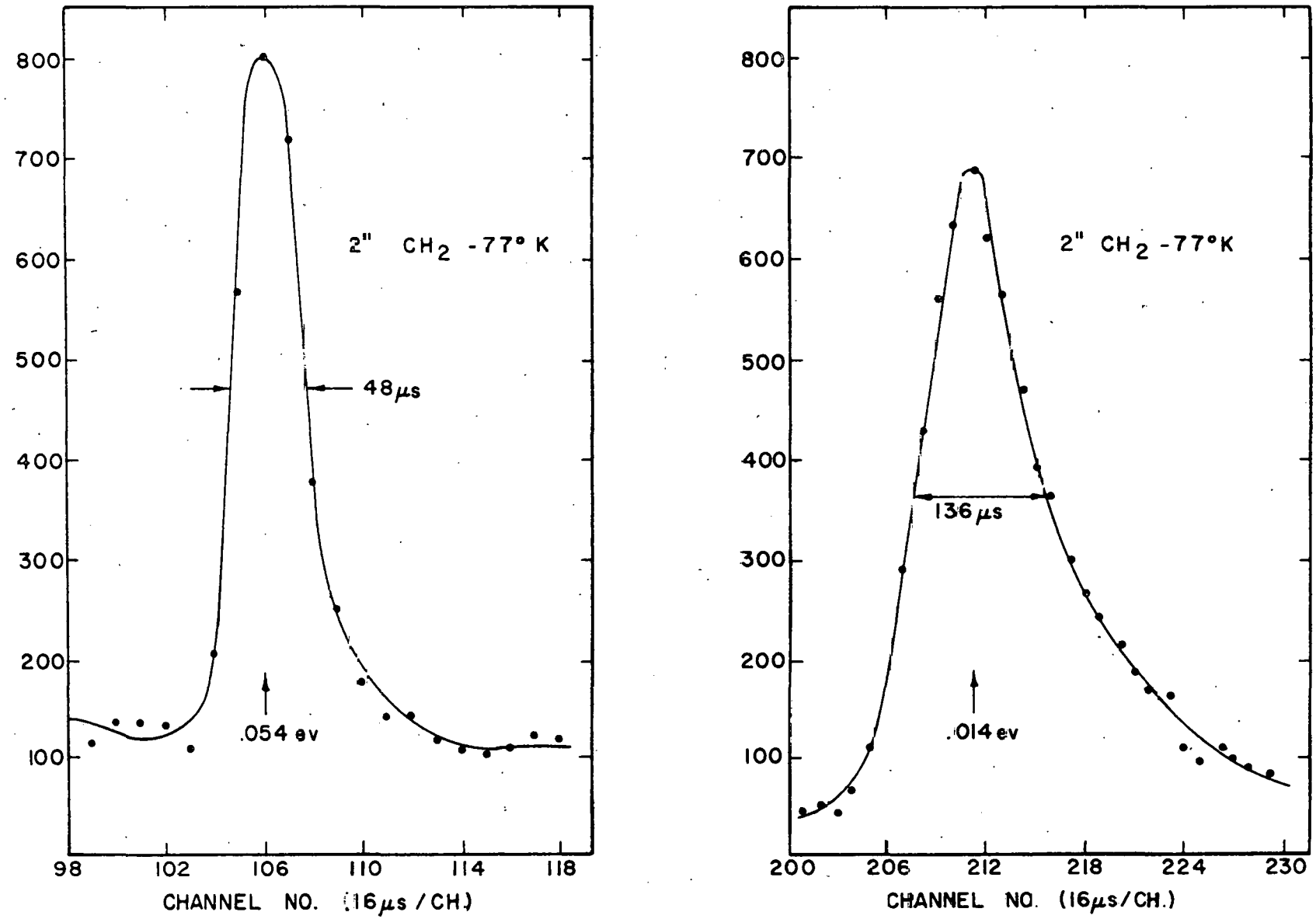

Fig. 6.--Emission times of neutrons selected by (111) planes in magnetite and produced by a 2-inch slab of polyethylene at 77°K

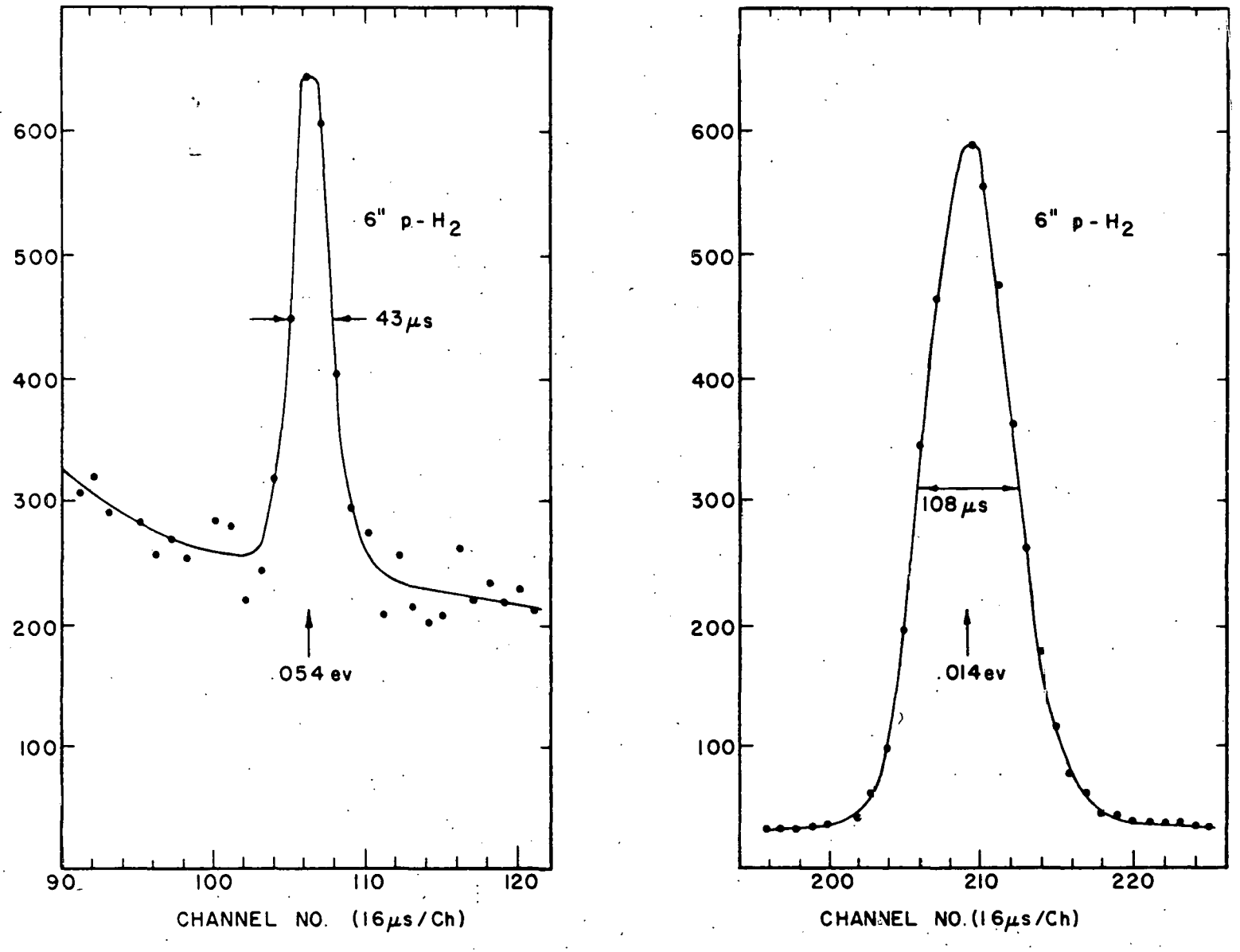

Fig. 7.--Emission times of neutrons selected by (111) planes in magnetite and produced by a 6-inch cylinder of para-hydrogen at 20.27°K

Small Neutron Chopper - Other investigations of the neutron emission times produced by a thin slab of moderator were carried out using a small neutron chopper having an aperture of 3/4 x 1-5/8 in. and an upper angular speed of 15000 rpm. Using a geometrical arrangement like that shown schematically in Fig. 8, a very short open time (~15μsec width at half maximum) for the chopper, and equal distances for source-to-chopper and chopper-to-detector legs ($L_1=L_2$), one will observe at the detector the exact time characteristics of the neutron source. Figure 9 illustrates how a neutron emission time of the shape shown will appear as a function of time at the detector. In a sense, the detected beam is a "mirror" image of the emitted beam. This technique has been applied to the study of neutron emission times from CH_2 at 77°K and to liquid para-hydrogen. Figures 10 and 11 show the results for a 2 in. layer of para-hydrogen and a 2 in. layer of CH_2 at 77°K. It is to be noted that the crystal technique gives results which agree very well with the chopper results.

In summary, one observes that the first element of the velocity selector can be made to give a time-dependent pulse roughly equivalent to that produced by a rotating neutron chopper usually used in a double chopper arrangement. The width at half maximum cannot be made much smaller than 45 μsec even with vanishing thickness for the slab moderator. The type and temperature of the slab of moderator are parameters which can be varied by the experimenter to achieve the best compromise in resolution and intensity. Table 2 summarizes this data for a number of typical cases of interest and also gives the relative intensity.

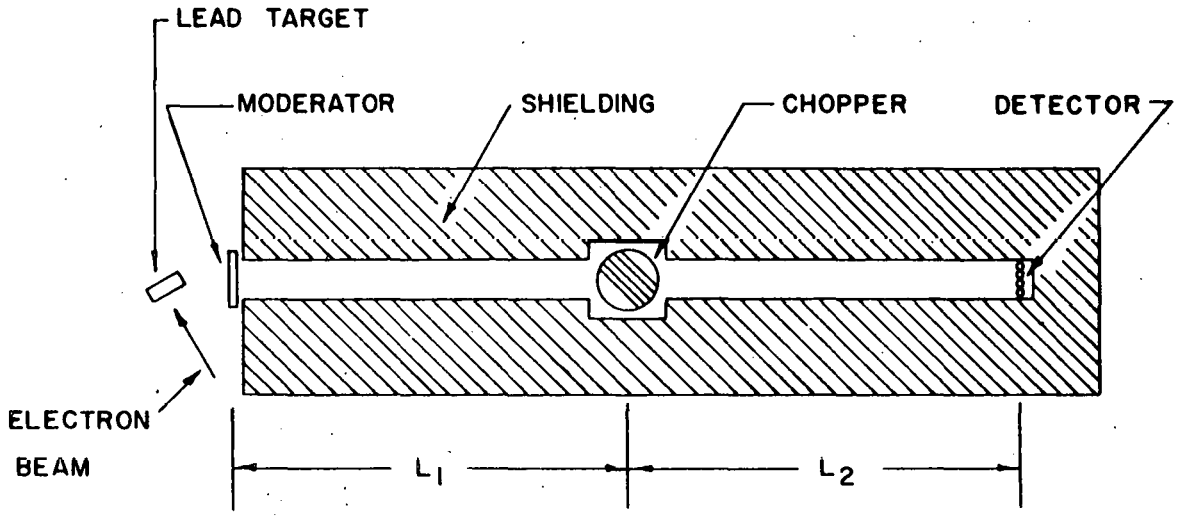

Fig. 8.--Schematic drawing of experimental arrangement to study neutron emission times using a small neutron beam chopper

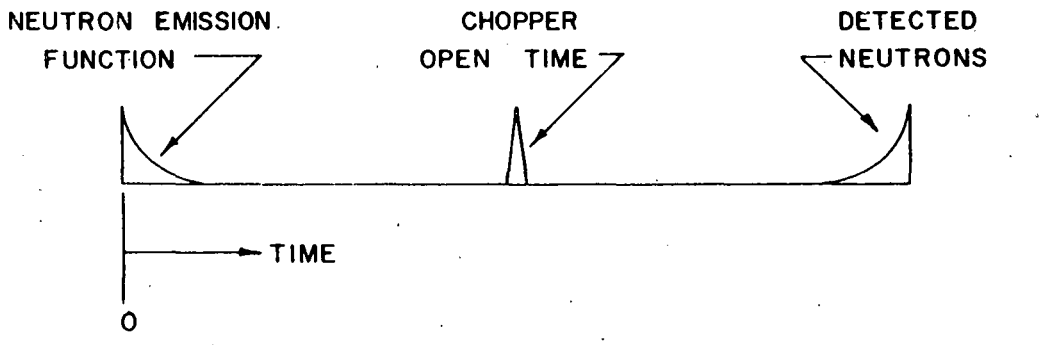

SOURCE - TO - CHOPPER DISTANCE = CHOPPER - TO - DETECTOR DISTANCE

Fig. 9.--Schematic drawing showing the relation of the time distribution of the detected neutrons to the neutron emission time for the case when the source-to-chopper distance equals the chopper-to-detector distance

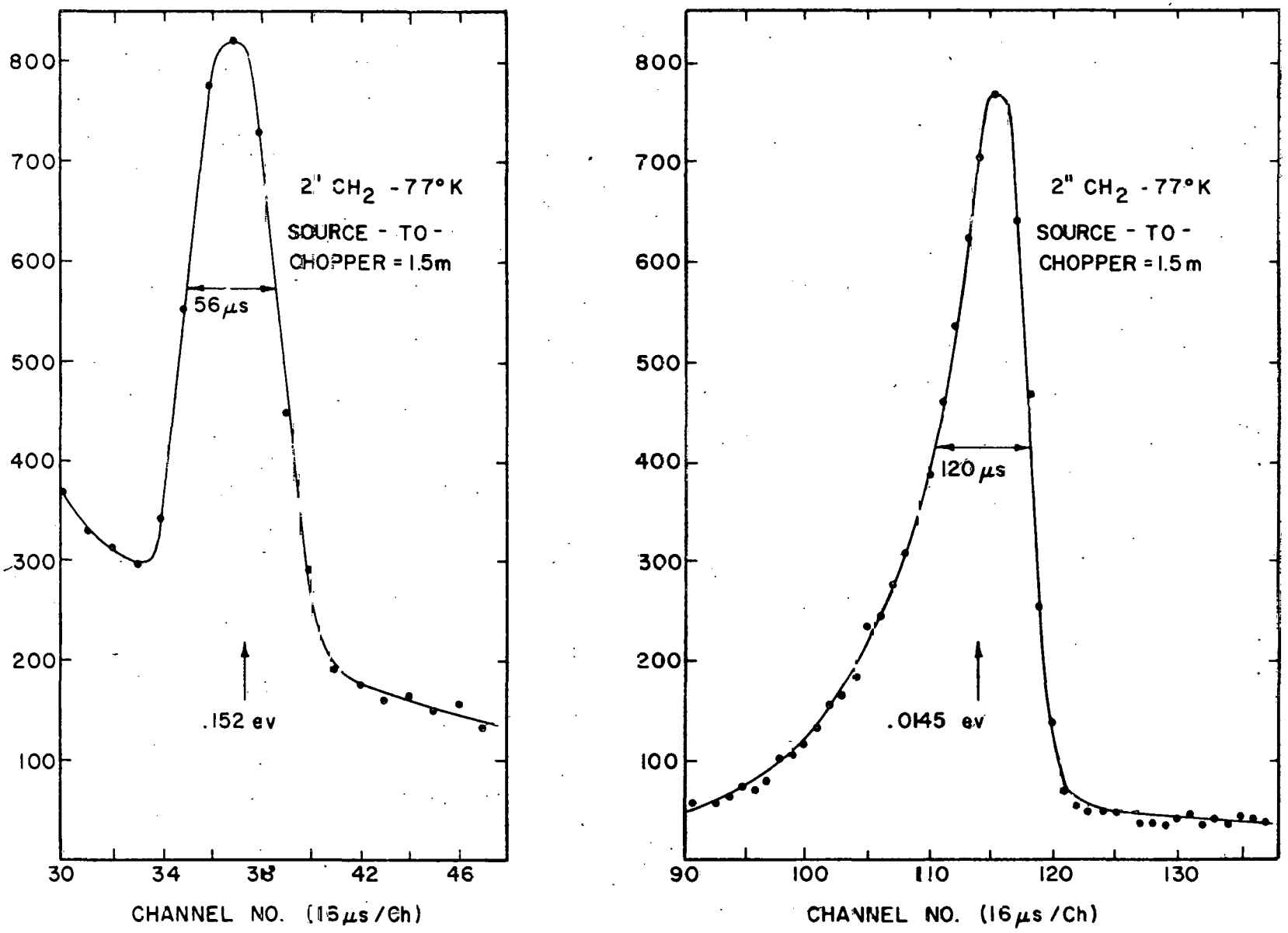

Fig. 10.--Observed neutron emission time using a small neutron beam chopper in an arrangement outlined in Figs. 8 and 9

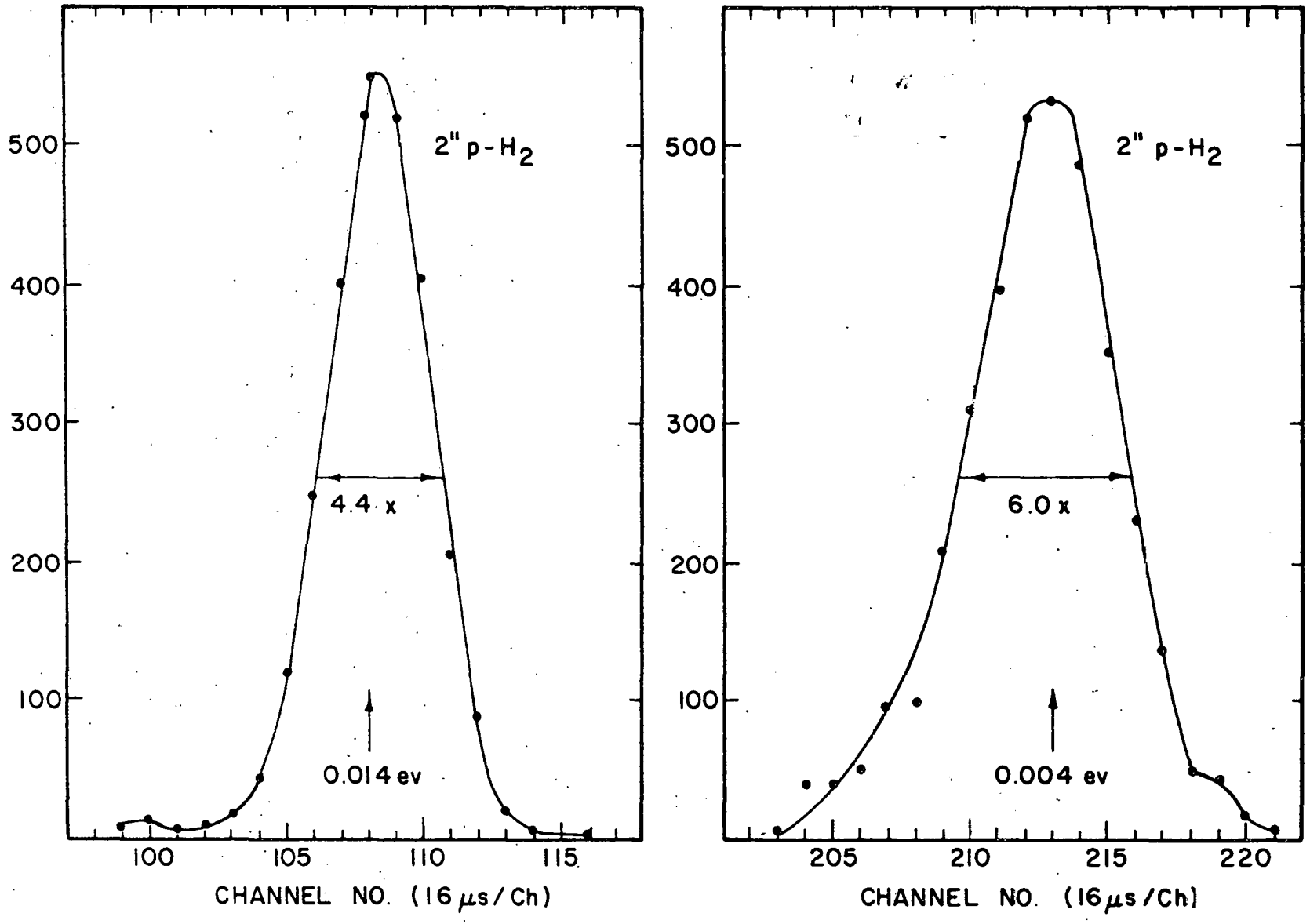

Fig. 11.--Neutron emission times from a 2-inch layer of para-hydrogen observed using a small rotating mechanical chopper

Table 2

COMPARISON OF THE FULL WIDTHS AT HALF HEIGHT FOR SELECTED THICKNESSES OF CH_2 AT 77°K AND LIQUID PARA-HYDROGEN

E (ev)	Liquid p-H_2						CH_2 - 77°K			
	Δ 2" (μsec)	N / B.P.	Δ 4" (μsec)	N / B.P.	Δ 6" (μsec)	N / B.P.	Δ 1" (μsec)	N / B.P.	Δ 2" (μsec)	N / B.P.
.004	6.0x16	0.45	7.5x16	1.0	11.0x16	1.3	9.2x16	0.25	15x16	0.56
.014	4.4x16	1.35	4.6x16	1.6	6.5x16	2.0	6.4x16	2.0	9.0x16	3.1
.034	5.0x16	0.78	4.1x16	0.8	4.0x16	0.93	4.8x16	1.8	6.5x16	2.5
.060	4.2x16	0.88	4.0x16	0.90	4.0x16	0.85	4.2x16	1.6	4.4x16	2.0

Note: The values in the column headed (N/B.P.) represent the total integrated counts N in the full width of curve for one beam pulse (B.P.). The counting rate data for para-hydrogen and polyethylene are directly comparable.

2.2 NEUTRON BEAM CHOPPER

The chopper used in the present experiments is a large aperture rotating-slit system of the Fermi type. The major consideration in the design of this chopper was the large aperture required for transmission of thermal neutrons. Figure 12 shows the stainless steel rotor which houses two identical slit systems. The diameter of the rotor is about 6 in. and its length is about 14 in. The irregular marks on the surface of the rotor are a result of dynamic balance adjustments. Figure 13 shows the rotating chopper in its steel housing (for personnel protection), and the series-wound one-horsepower motor. In the bottom slot one sees a slit assembly. At present, two different slit systems are available; one is a set of parallel slits, while the other is a set of curved slits with 24 in. radius. The one-horsepower series-wound motor is mounted coaxially with the chopper and joined to it by a flexible coupling. The no-load upper speed limit of the motor is about 12,000 rpm. With about 120 volts applied, this motor is able to bring the chopper to a speed slightly in excess of 10,800 rpm. This corresponds to a rotational

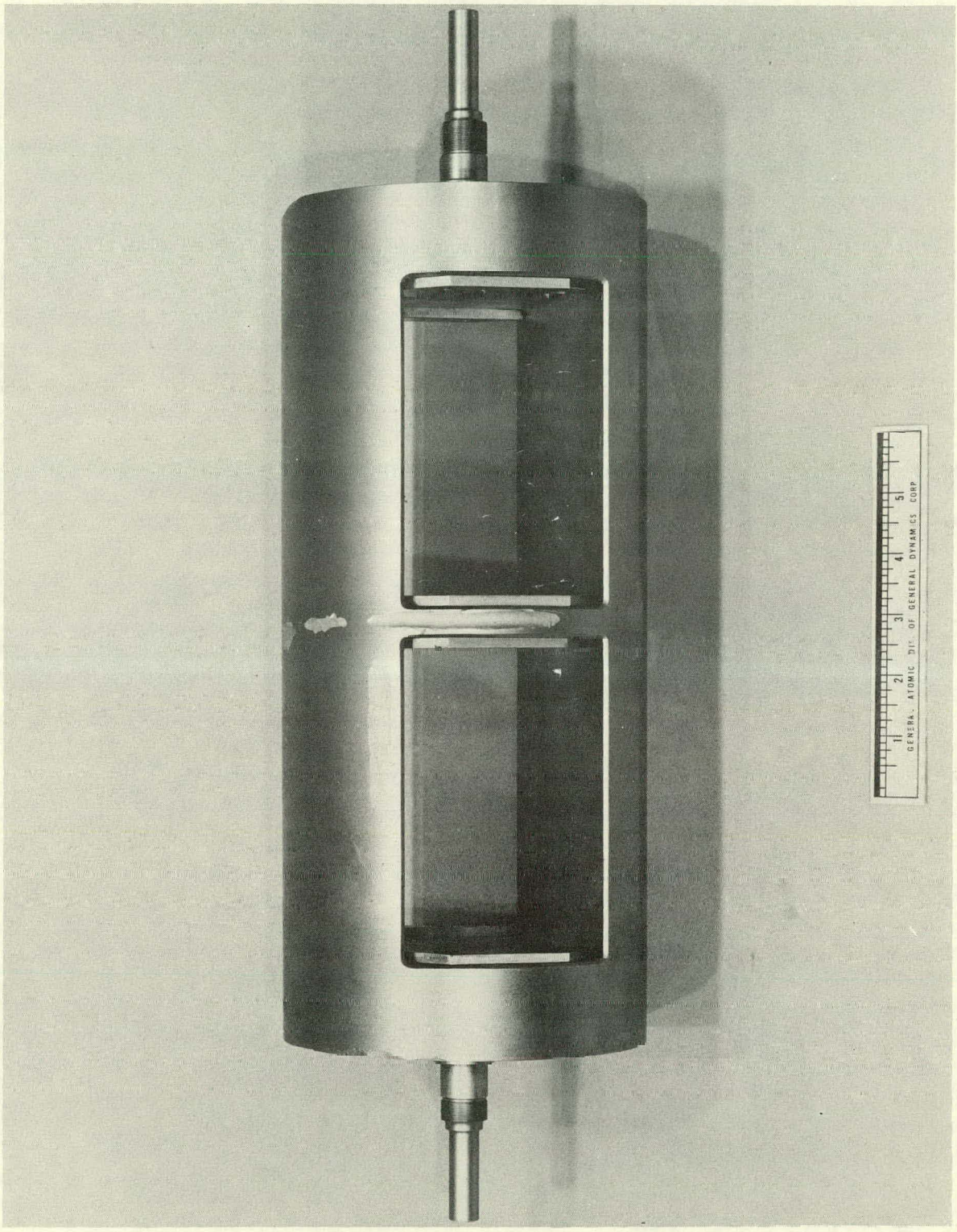

Fig. 12 -- Stainless steel rotor for slow neutron chopper

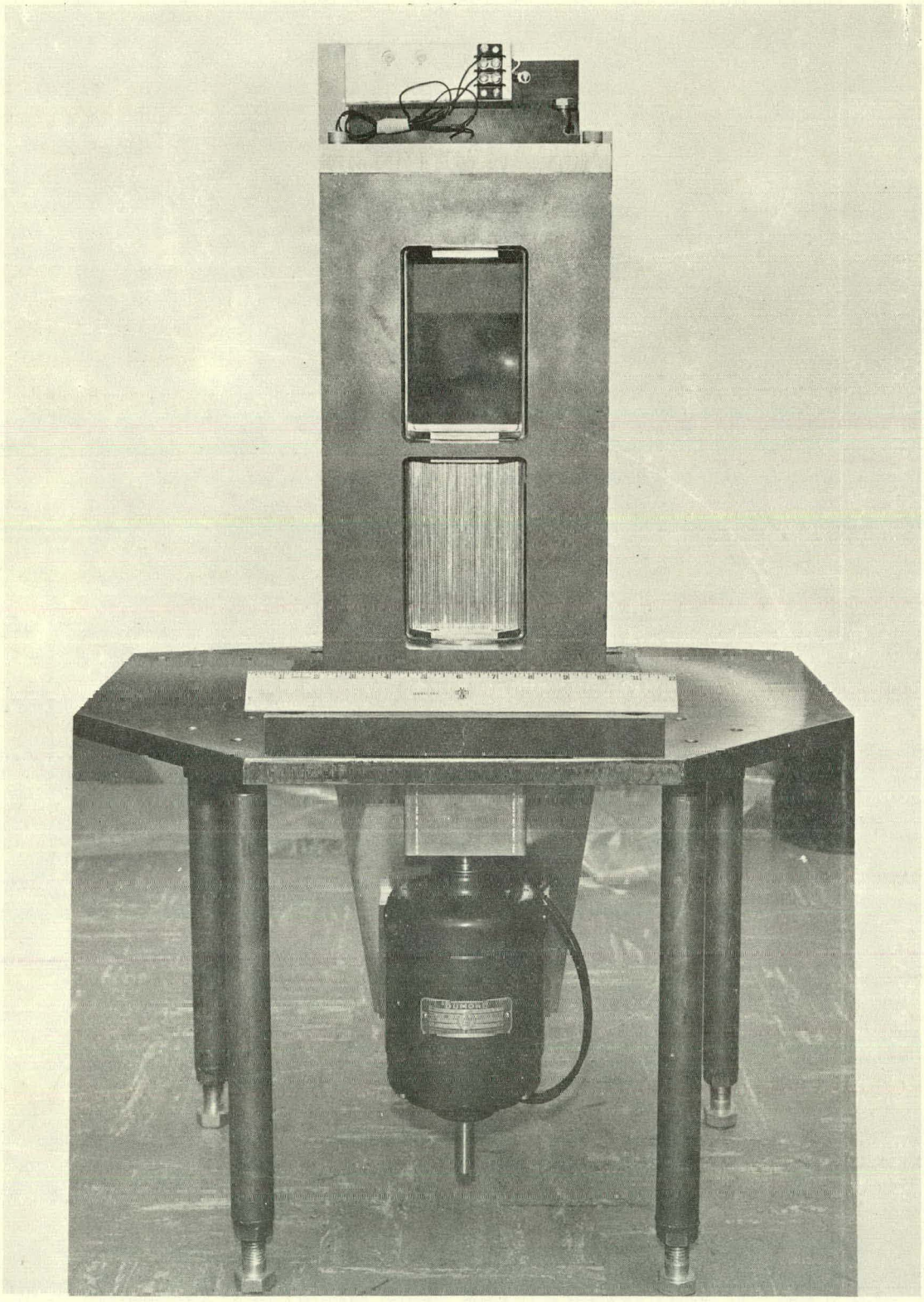

Fig. 13 -- Slow neutron chopper (The bottom slot contains a "sandwich" of narrow defining slits)

speed of 180 pulses per second (pps), the linear accelerator repetition rate required in order to produce maximum power output. The chopper and motor are operated in normal air pressure. The top and bottom bearing plates are individually water cooled to lengthen the life of the thrust ball bearings.

The individual chopper slit assembly is made as a single unit which slides into a slot in the rotor. Both the straight and curved slits are fabricated from alternating layers of absorber and spacer. The aluminum spacers are thinly ribbed but have sufficient mechanical strength against the centrifugal forces and, on the average, present a maximum of 1/2 in. of aluminum to the transmitted neutrons. The absorber is a 0.009-in. nickel sheet with 0.001 in. of cadmium plated on each side. A many layered "sandwich" is made from a number of these alternating layers and is bolted securely between two quarter-inch steel side plates. The whole assembly is then machined accurately to fit with close tolerances into the slots in the chopper. To form the curved slits, the two side plates have mating 24-in. radii on their adjacent interior surfaces. The sandwich assembly is then pressed between these two curved slits and securely bolted.

The individual aluminum spacers are 0.050 in. thick and the length of the chopper slits is 4.0 in; consequently the angular aperture of an individual slit is 0.025 rad. The width and length of the rotating slit, together with the rotational angular velocity of the slit assembly, operate so as to introduce a lower neutron-velocity limit called the cutoff velocity, v_c. This cutoff velocity is given by: $v_c = \omega R^2/h$ where R is the radius of the slit system and h is the separation of the slits. Table 3 shows the manner in which the neutron cutoff velocity varies with the angular rotational speed for the present system.

Table 3

TIIE DEPENDENCE OF THE CUTOFF VELOCITY, v_c, ON THE CHOPPER ROTATIONAL SPEED f

f (cps)	v_c (m/sec)	$10^6/v_c$ (μsec/m)	E_c (ev)
60	754	1326	0.003
90	1131	884	0.00675
120	1508	663	0.012
180	2262	442	0.027

For neutrons of lower velocity, the slit system must be curved to increase the effective transmission of the chopper. A relation between the neutron velocity, v_c, the angular rotation ω, and the required radius ρ of such curved slit is given by $V_o = 2 \omega \rho$. For the present curved-slit system and with $\rho = 24$ in., the maximum transmission of the chopper occurs for neutrons with energies of 0.0044 ev when the rotational speed is 120 rps, and for neutrons with energies of 0.0099 ev when the rotational speed is 180 rps. It has been shown by calculation that the transmission function is rather flat and slowly varies around the maximum. Consequently, neutrons with energies of two to three times the energy of maximum transmission can be obtained effectively with this chopper. We are thus able to use either the curved or the straight slits to cover reasonably effectively the entire spectrum of neutron energies from 0.005 ev up to 0.250 ev. If a substantial number of runs are needed with the best time resolution for neutron energies in the range 0.030 ev, an additional set of curved slits with a longer radius will be required.

2.3 DETECTORS

The detectors for this experiment consist of 1-in. diameter BF_3 proportional counters. The boron gas is fully enriched in B^{10} and the effective length is 18 inches. In order to maximize the efficiency, the pressure of the filling gas is about 1.6 atmospheres (stp). At present the individual banks of counters are formed from nine 1-in. counters, close packed in two layers with the five-counter layer closest (160 cm) to the scatterer. Since an individual circular counter of radius R presents an average path length to the incident beam of $\pi R/2$, the transmission ratio of such a counter for neutrons of 0.025 ev is ~ 0.72. Such a counter is therefore quite "thin."

The angular coverage by the detector bank is governed mainly by the area of the detector. For the 5 x 18 in. detector bank, the angle subtended is about 4 deg in the horizontal and 16 deg in the vertical direction. For some measurements, particularly at 90 deg, the angular divergence in the horizontal can be made larger without loss of resolution. The large vertical angular divergence is satisfactory since most scattered beams are axially symmetric.

2.4 VELOCITY SELECTOR

The arrangement of the various components, just described, has been shown in Fig. 2. The pertinent dimensions and parameters of the system now in use are as follows:

neutron source-to-chopper distance	2.77 meters
chopper-to-scatterer distance	0.26 meters
scatterer-to-detector distance	1.59 meters
neutron chopper aperture	2-3/4 x 10 in^2
chopper rotational speed, f	0 - 180 pps.
elementary chopper slit dimensions	0.050 ft x 4.0 in.
elementary slit aperture, α_1	0.025 rad.
Soller slit angular aperture, α_2	0.01, 0.02, and 0.04 rad as desired
peak linear accelerator current	0.500 - 0.600 amp
Linear accelerator electron energy	28 Mev

The chopper and the Soller slit, together with the rotating speed f, determine the chopper open time, $t_{\frac{1}{2}}$ (defined as the pulse width at half maximum) according to the relation:

$$(\alpha_1 + \alpha_2) = 2\omega t_{\frac{1}{2}}$$

From this one predicts that for a rotational speed of 180 rps, $t_{\frac{1}{2}} \sim 20$ μsec for $\alpha_2 = 0.02$ rad. The Soller slit is very useful here because the angular aperture of the collimator without the Soller slit assembly is about 0.06 rad. Without the Soller slit, the pulse width, $t_{\frac{1}{2}}$, would be ~ 38 μsec, clearly a much poorer arrangement for good time resolution.

The arrangement for the velocity selector just discussed has been used for a variety of measurements on inelastic neutron scattering. A typical overall time resolution measurement is shown in Fig. 14 where the neutrons were scattered from a thin vanadium scatterer into the detector set at a scattering angle of 90 deg. Here the time resolution $\Delta T/T$ is seen to be about 0.08 for $E_o = 0.089$ ev. The flight time T is for the flight path from the scatterer to the detector bank. This particular flight path is used to be in agreement with measurements on inelastically-scattered neutrons which gain or lose energy in the scatterer.

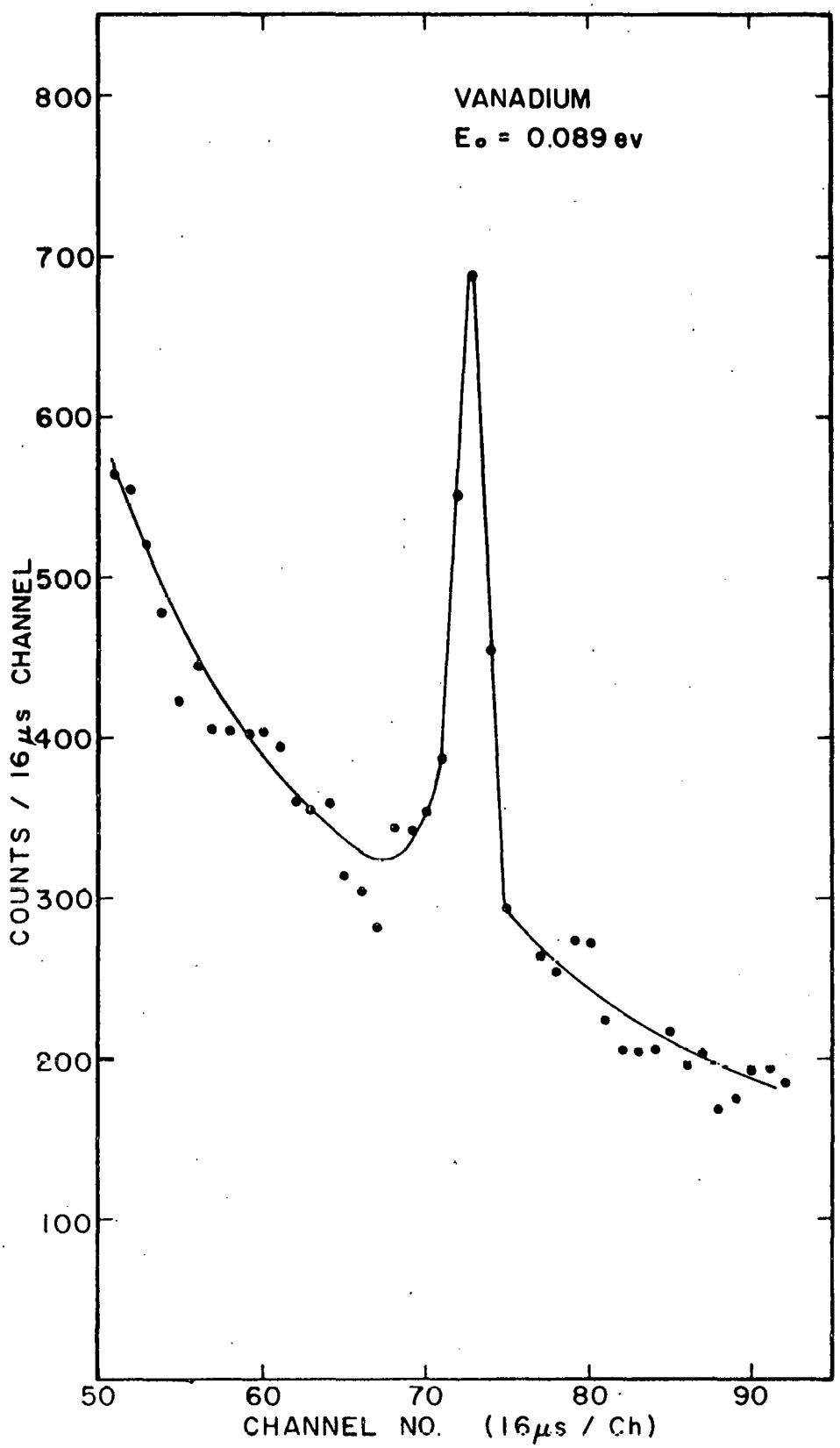

Fig. 14.--An experimental measurement of the time resolution for the neutron velocity selector

III. NEUTRON INTERACTIONS IN LIQUID PARA- AND ORTHO-HYDROGEN

Preliminary measurements made last year[1] indicated that the neutrons interact differently in para-hydrogen than in other hydrogeneous substances. The total scattering cross section for para-hydrogen showed strong evidence for the para-to-ortho-transistion (0 → 1) at 0.015 ev. During this reporting period several improved measurements were made, both on the total scattering cross section and on the inelastic scattering of neutrons by thin layers of para- and ortho-para-hydrogen. The interactions have been analyzed in terms of a "perfect gas" model in which the individual molecules of hydrogen are not subjected to the influence of neighboring atoms. Sarma[3] has published for this latter problem a complete treatment which will be compared extensively with the experimental data.

3.1 THEORY OF NEUTRON SCATTERING IN A PERFECT HYDROGEN GAS

Sarma's treatment of the scattering of low energy neutrons from liquid hydrogen utilizes the formalism of Van Hove[4] to describe, in Born approximation, the scattering by a system of particles subject to the assumptions that the Hamiltonian is independent of the spins, and that there are no correlations between the position and orientation of a particular molecule nor between the orientations of different molecules. Moreover, the hydrogen molecule is approximated by a simple rigid rotator and thus possesses the rotational states

$$E_J = (\hbar^2/ma^2)\, J\,(J+1) = 0.015\,(J/2)\,(J+1)\ \text{ev} \qquad (1)$$

where m is the proton mass and a (0.75 Å) is the distance between the two protons in the hydrogen molecule. Consideration of the vibrational modes is neglected since the incident neutron energies in the range of interest are much smaller than the minimum energy necessary to excite the lowest of these modes.

With these assumptions, the differential cross-sections for "coherent" and "incoherent" scattering are found to be

$$\frac{d^2\sigma}{d\Omega dE} = \frac{2N}{\pi} \frac{k}{\hbar k_o} 4A_{coh}^2 \sin^2 \int e^{i(\bar{K}\bar{r} - \omega t)} G_d(\bar{r}, t)\, d\bar{r}\, dt \qquad (2)$$

and

$$\frac{d^2\sigma}{d\Omega dE} = \frac{2N}{\pi} \frac{k}{\hbar k_o} f_{J\to J'} \frac{Ka}{2} \int e^{i\left[\bar{K}\bar{r} - (\omega - \frac{E_{J'} - E_J}{\hbar}) t\right]} G_s(\bar{r}, t)\, d\bar{r}\, dt \qquad (3)$$

respectively. In these expressions N is the number of molecules, A_{coh} is the coherent scattering length of the proton, and $\bar{K} = \bar{k} - \bar{k}_o$. Here, $\bar{k}_o$ and $\bar{k}$ are the neutron wave vectors before and after scattering. $G_d(\bar{r}, t)$ and $G_s(\bar{r}, t)$ are the "distinct" and "self" parts of Van Hove's pair distribution in space and time $G(\bar{r}, t)$, which in its classical limit gives the probability of finding an atom at position $\bar{r}$ and time t, given an atom at the origin at time zero. The separation of $G(\bar{r}, t)$ into "self" and "distinct" parts distinguishes whether the atom at $\bar{r}, t$ is the same or a different atom from the one assumed to be at the origin at time zero.

The use of quotation marks around "coherent" and "incoherent" notes the fact that Eqs. (2) and (3) do not describe the coherent and incoherent cross-sections in the usual sense. Van Hove has shown that the coherent differential cross-section is the 4-dimensional Fourier transform of the function $G(\bar{r}, t)$, whereas in Eq. (2) only the "distinct" part of this function appears. Thus Eq. (2) accounts only for that part of the coherent scattering arising from different molecules and contributes little to the observed scattering due to the small numerical values of A_{coh} and $G_d(\bar{r}, t)$.

That portion of the coherent scattering omitted in Eq. (2) is included in Eq. (3), so that the latter accounts not only for the incoherent scattering but also for the coherent scattering resulting from the neutron's interaction with individual molecules. The term $f_{J\to J'}$ is a function of Ka/2 (and therefore a function of angle) and its value depends strongly on the initial and final states of the hydrogen molecule, i.e., upon the transition considered. In the para and ortho modifications of liquid hydrogen, all of the molecules are assumed to be in their lowest states (J = 0 and J = 1, respectively). Thus for incident neutron energies less than 0.1 ev, the following are the only values of $f_{J\to J'}$ that need be considered.

$$f_{o\to o} = 4\ p_o\ A^2_{coh}\ B_o^2$$
$$f_{o\to 1} = 12\ p_o\ A^2_{incoh}\ B_1^2$$
$$f_{1\to 1} = 4\ p_1\ (A^2_{coh} + 2/3\ A^2_{incoh})\ (B_o^2 + 2\ B_2^2) \qquad (4)$$
$$f_{1\to o} = (4/3)\ p_1\ A^2_{incoh}\ B_1^2$$
$$f_{1\to 2} = (4/3)\ p_1\ A^2_{incoh}\ (2B_1^2 + 3B_3^2)$$

Here p_J is the statistical weight of the molecules in the state J and the B's are spherical Bessel functions of the argument Ka/2. These values of f can differ by several orders of magnitude because of the difference in the values $A^2_{coh} = 3.57 \times 10^{-2}$ barns and $A^2_{incoh} = 1.59$ barns.

Direct application of Eq. (3) depends on the form of $G_s(\bar{r},t)$. As a first approximation, Sarma considers the case where intermolecular forces may be neglected and takes for $G_s(\bar{r},t)$ the autocorrelation function of a perfect gas, i.e.:

$$G_s(\bar{r},t) = \left[\frac{2\pi t(k_B T t - i\hbar)}{2m}\right]^{-3/2} \exp - 2mr^2/2t(k_B T t - i\hbar) \qquad (5)$$

With this model the differential "incoherent" scattering cross-section becomes

$$\frac{d^2\sigma}{d\Omega dE} = \left(4\ \frac{m}{\pi k_B T}\right)^{1/2} \frac{k}{\hbar k_o}\ \frac{f_{J\to J'}}{K} \exp - m\ \frac{\left[\hbar\omega - (E_{J'} - E_J) - \frac{\hbar^2 K^2}{4m}\right]^2}{k_B T \hbar^2 K^2} \qquad (6)$$

The numerator of the exponent expresses the conservation of energy in terms of the energy transfer $\hbar\omega - (E_{J'} - E_J)$ and the momentum transfer hK. Expressing these in terms of energy, i.e.:

$$\hbar\omega - (E_{J'} - E_J) = E_o - E - (E_{J'} - E_J)$$
$$\hbar^2 K^2 = 2m\ (E + E_o - 2\sqrt{EE_o}\cos\varphi) \qquad (7)$$

where Eo, and E are the initial and final energies of the neutron and φ is the angle of scattering, Eq. (6) can be rewritten

$$\frac{d^2\sigma}{d\Omega dE} = \frac{4(2\pi k_B T)^{-1/2}(E/E_o)^{1/2}(f_{J\to J'})}{\left[E + E_o - 2\sqrt{EE_o}\cos\varphi\right]^{1/2}} \exp - \frac{9\left[\frac{1}{3}(E_o - 2\Delta E_{J'J} + 2\sqrt{EE_o}\cos\varphi) - E\right]^2}{8\,k_B T\,(E+E_o-2\sqrt{EE_o}\cos\varphi)} \quad (8)$$

Thus, $\frac{d^2\sigma}{d\Omega dE}$ takes on its maximum value when

$$E = 1/3\,(E_o - 2\Delta E_{J'J} + 2\sqrt{EE_o}\cos\varphi) \quad (9)$$

in agreement with what one would expect from simple classical considerations. The exponential term in Eq. (8) describes an intrinsic broadening associated with each of the scattering components and, as a consequence of the initial assumptions, this broadening is due entirely to the thermal motions of the hydrogen molecules.

Inasmuch as all of our data, thus far, has been obtained with $\varphi = 90$ deg, further consideration will be limited to this special case. Equation (8) then reduces to

$$\left.\frac{d^2\sigma}{d\Omega dE}\right|_{\varphi=\pi/2} = 4(2\pi k_B T)^{-1/2}\left(\frac{E}{E_o}\right)^{1/2}\frac{f_{J\to J'}}{(E+E_o)^{1/2}}\exp - \frac{9\left[\frac{1}{3}(E_o - 2\Delta E_{J'J}) - E\right]^2}{8\,k_B T(E+E_o)} \quad (10)$$

If the average energy after scattering,

$$\bar{E} = 1/3\,(E_o - 2\,\Delta E_{J'J}) \quad (11)$$

is assigned to all values of E except in the numerator of the exponent, the right hand side of Eq. (10) is a simple Gaussian with its full-width at half-maximum given by

$$\delta\xi = (4/3)\,(2k_B T \ln 2)^{1/2}\,(E+E_o)^{1/2} = 2.4\,(E_o - \Delta E_{J'J}/2)^{1/2}\text{mev} \quad (12)$$

To the same degree of approximation and letting $\epsilon = 1/3\,(E_o - 2\Delta E_{J'J}) - E$, we can integrate Eq. (10) obtaining

$$\left.\frac{d\sigma}{d\Omega}\right|_{\varphi=\pi/2} = 4\left(\frac{1}{2\pi k_B T}\right)^{1/2}\left(\frac{E}{\bar{E}}\right)^{1/2}\frac{f_{J\to J'}}{(E+E_o)}\,1/2\int_{\infty}^{\infty}\exp - 9\epsilon^2/8k_B T(E+E_o)\,d\epsilon \quad (13)$$

$$= \frac{8}{3}\left(\frac{E_o - 2\Delta E_{J'J}}{3E_o}\right)^{1/2} f_{J\to J'}\left(\frac{K_a}{2}\right)$$

where the argument Ka/2 has the value 0.3 $(E_o - \Delta E_{J', J}/2)^{1/2}$ when the energies are expressed in milli-electron volts (mev).

The broadening $\delta \xi$ depends both on the incident neutron energy and on the transition considered. This dependence is shown in Fig. 15 where the energy broadening for 90 deg scattering is plotted as a function of E_o for the various scattering components. It is seen that in all cases the broadening is quite large for all but the lowest incident energies. The dotted portions of the two lower curves represented the energy ranges where the incident neutron energy is insufficient to excite these transitions.

In applying Eq. (13) to the case of para-hydrogen, it is necessary to consider only the two scattering components associated with the transitions $0 \rightarrow 0$ ("elastic") and $0 \rightarrow 1$. By substituting the appropriate values of $f_{J \rightarrow J'}$ from Eq. (4), with $p_o = 1$, into Eq. (13), the magnitudes of the differential cross-sections at $\varphi = 90$ deg for these scattering components are easily calculated. The results are shown in Fig. 16 as a function of the incident neutron energy. The elastic component is proportional to A^2_{coh} and is so small that ten times its value has been plotted. It is of interest to note that both cross-sections go to zero for particular values of E_o. Fig. 17 shows a similar plot of the differential cross-sections evaluated at $\varphi = 90$ deg for the various components scattered from ortho-para-hydrogen. In this case all of the transitions listed in Eq. (4) are possible and the curves shown were calculated assuming a 2:1 ortho-to-para mixtures (i.e., $p' = 0.67$ and $p_o = 0.33$).

It should be noted that the approximations made in the derivation of Eqs. (12) and (13) are not generally valid. When $E \rightarrow 0$ or when its value is small and comparable with the expected broadening, the representation of a scattered component as a simple Gaussian is not sufficiently accurate. In such cases an exact evaluation of Eq. (7) has been made in comparing theory with the experimental results. An example of such an analysis is shown in Fig. 18 where the scattering components, $(0 \rightarrow 1)$, $(1 \rightarrow 0)$, $(1 \rightarrow 2)$, and $(0 \rightarrow 0), (1 \rightarrow 1)$, are exhibited for 0.065-ev neutrons incident on ortho-para-hydrogen.

3.2 MEASUREMENTS ON INELASTIC SCATTERING OF NEUTRONS BY LIQUID HYDROGEN

For the present measurement, the apparatus outlined above has been used to select those incident energies which minimize one or more of the scattering components. In order to facilitate the discussion these energies are summarized in Table 4. In the case of para-hydrogen the scattering is effectively due to a single component for the incident

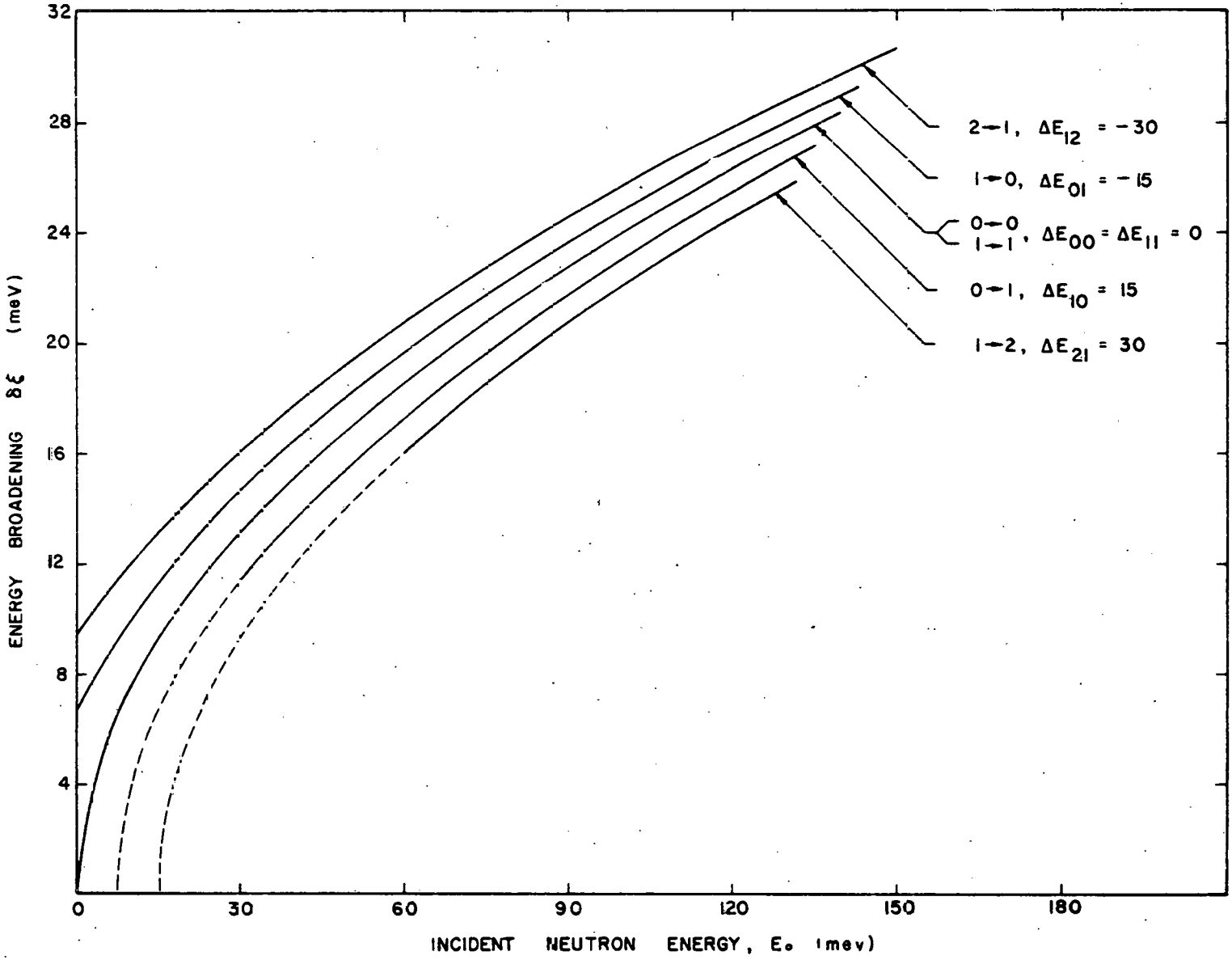

Fig. 15.--A plot of the theoretical broadening of the energy distribution of neutrons scattered at 90 deg

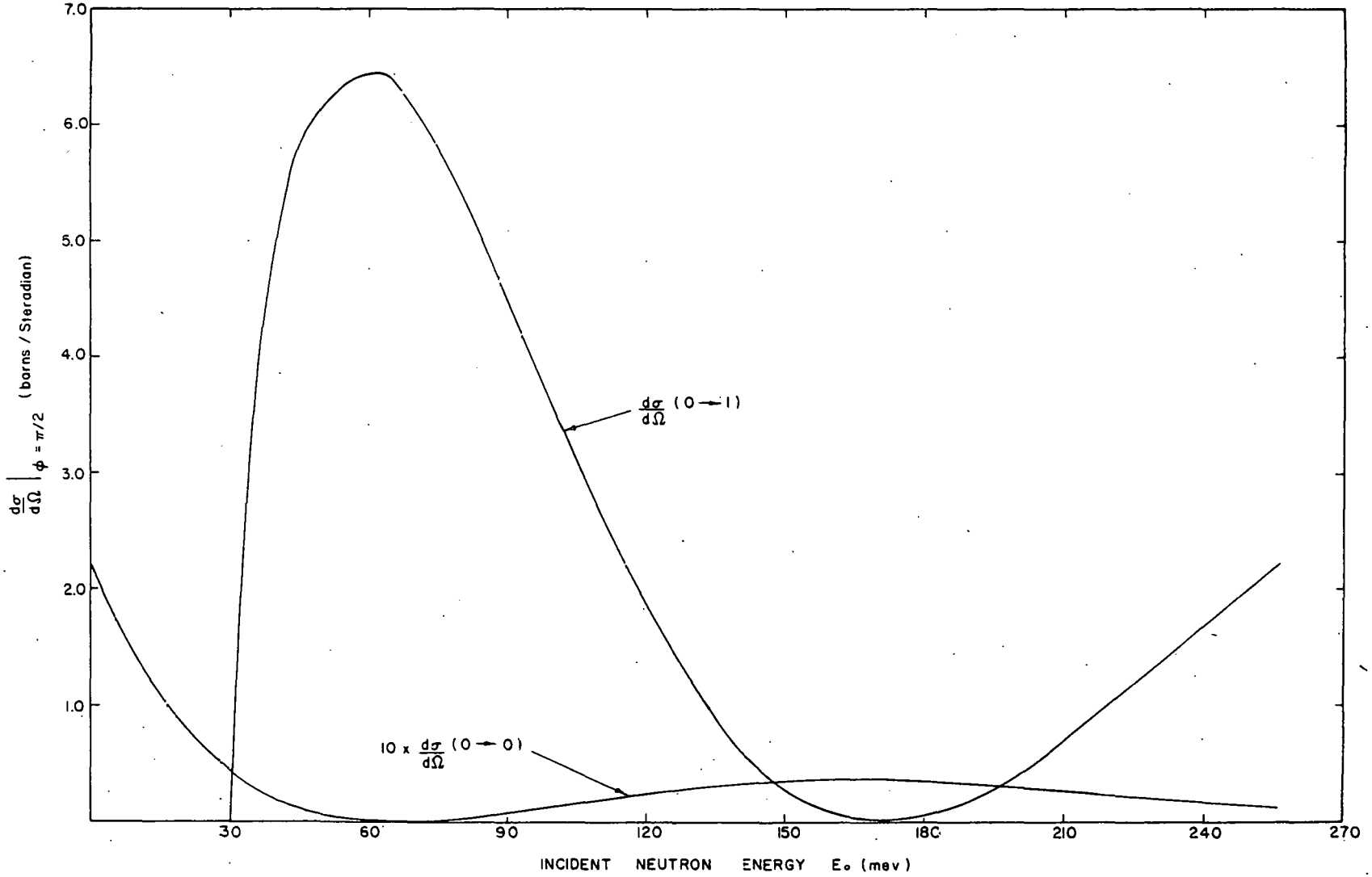

Fig. 16.--The differential cross sections evaluated at φ=90 deg for the (0 → 0) and (1 → 1) scattered components from para-hydrogen

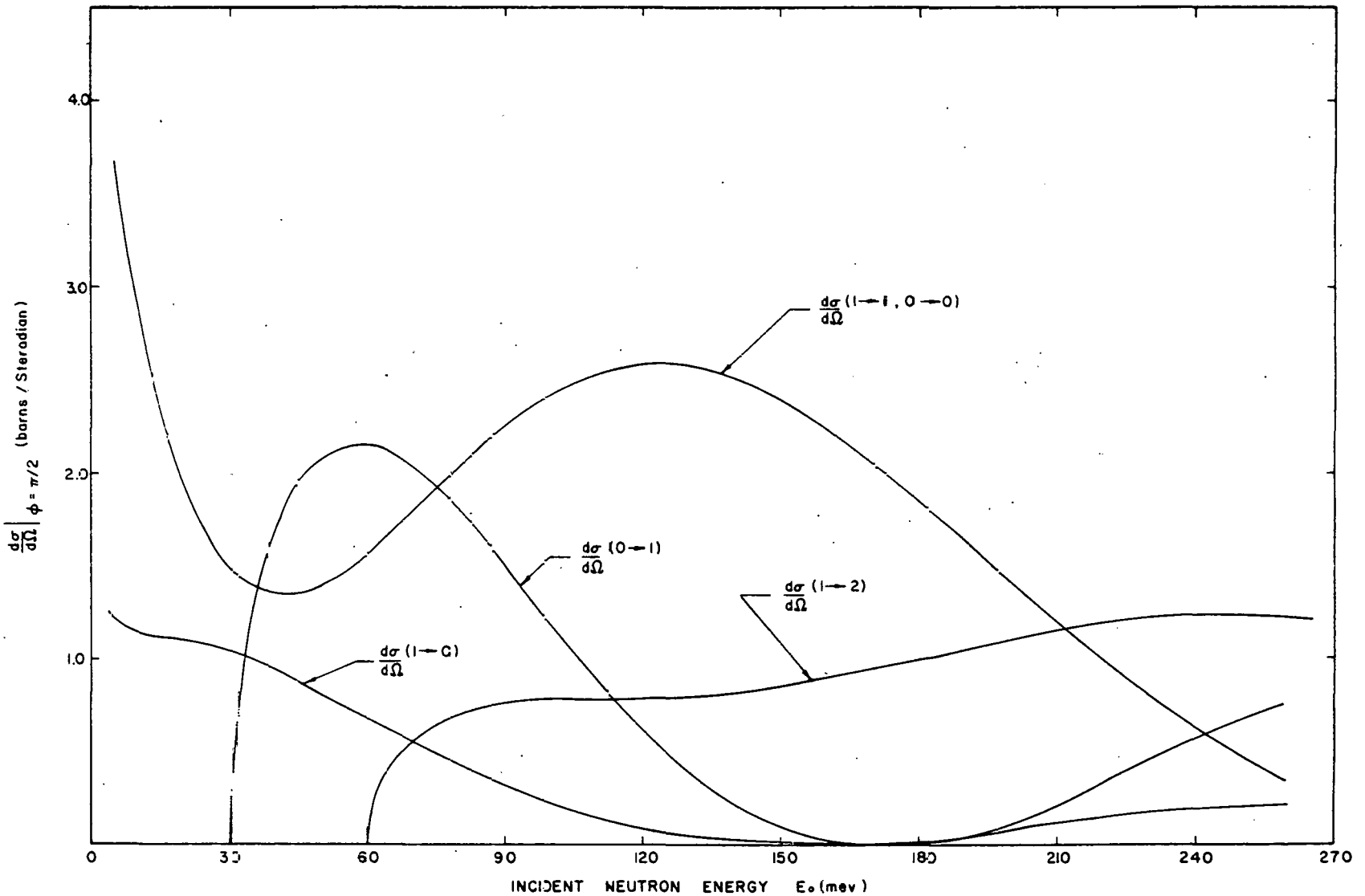

Fig. 17.--The differential cross sections evaluated at φ = 90 deg for the various scattering components from a mixture of 2:1 ortho-para-hydrogen

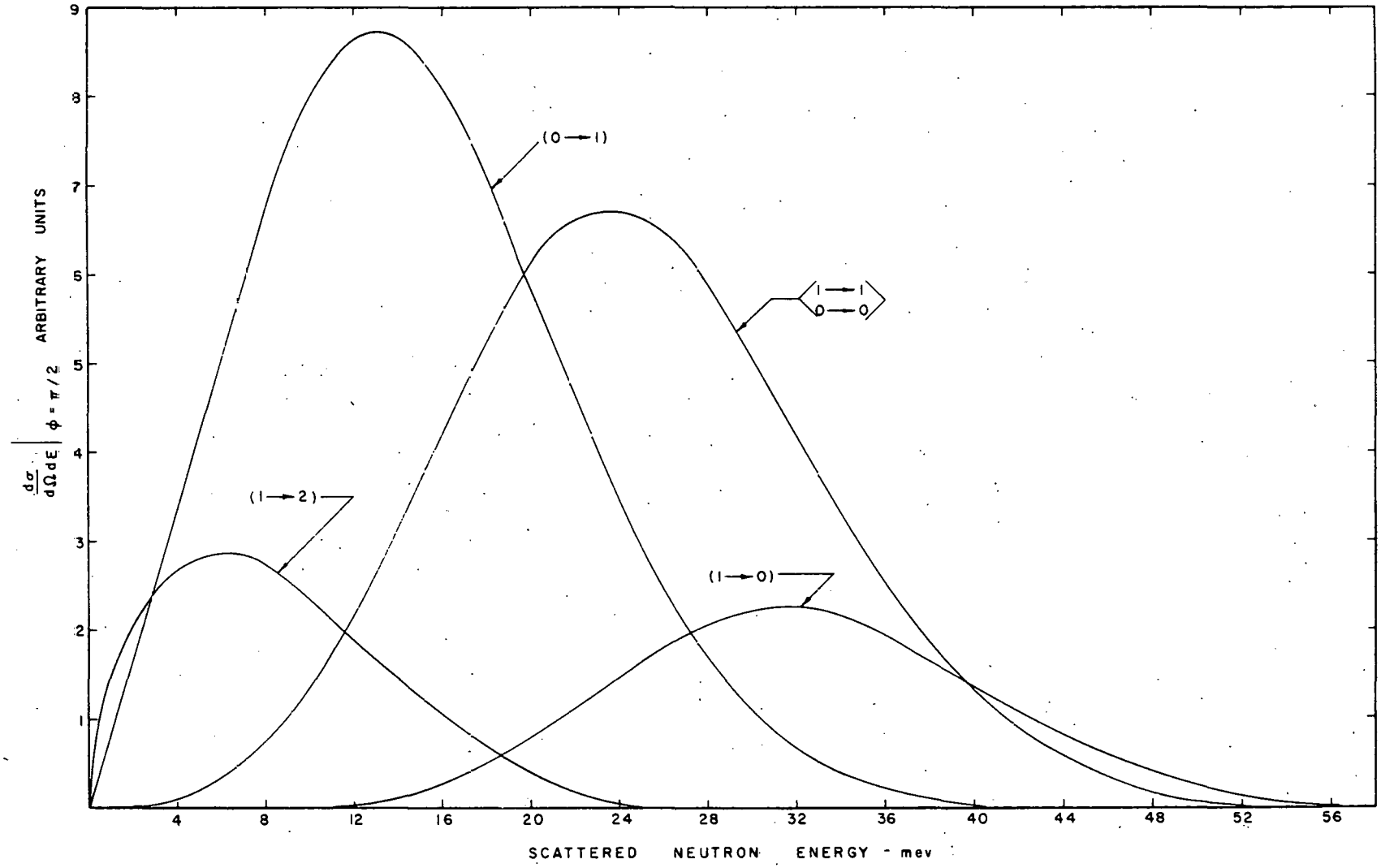

Fig. 18.--The four components of the scattering from a mixture of ortho-para-hydrogen at 90 deg for neutrons with E_o = 65 mev

energies chosen. For $E_o < 0.030$ ev the neutron energy is insufficient to excite the first rotational level while above this threshold the $(0 \rightarrow 1)$ level is predominant due to the very small cross-section of the "elastic" $(0 \rightarrow 0)$ scattering. The situation with ortho-para-hydrogen is more complicated since at least one inelastic component is present in addition to the "elastic" $(0 \rightarrow 0,\ 1 \rightarrow 1)$ scattering.

Table 4

SELECTED OPTIMUM INCIDENT ENERGIES, E_o, TO ELIMINATE CERTAIN CONTRIBUTIONS TO THE SCATTERING AT 90 DEG FROM VARIOUS ROTATIONAL LEVELS IN LIQUID HYDROGEN

Scatterer	E_o (ev)	Contributions
p-H	< 0.030	$0 \rightarrow 0$
	~ 0.065	$0 \rightarrow 1$
	~ 0.170	$0 \rightarrow 0$
o-p-H	< 0.030	$1 \rightarrow 1,\ 0 \rightarrow 0,\ 1 \rightarrow 0$
	$0.030 < E_o < 0.060$	$1 \rightarrow 1,\ 0 \rightarrow 0,\ 1 \rightarrow 0,\ 0 \rightarrow 1$
	~ 0.170	$1 \rightarrow 1,\ 0 \rightarrow 0,\ 1 \rightarrow 2$

The instrumental resolution was measured over the range of incident energies employed by measuring the elastic scattering from a thin sheet of vanadium. ΔT is the width at half maximum for the observed scattered distribution and T is the flight time for the flight path from the scatterer to the detector. The values found for $\Delta T/T$ vary between 0.05 and 0.10 depending upon the exact experimental conditions; i.e., chopper speed, beam divergence, and moderator used as the neutron source. Although the resolution is inadequate for many applications, it is satisfactory in the case of liquid hydrogen due to the large intrinsic thermal broadening associated with the various scattering components. Finally, the calibration of the energy scale was determined by measuring the different flight times for elastic scattering from vanadium over different known flight paths with other experimental conditions held constant.

Figure 19 shows the measured distribution of initially monoenergetic 0.065-ev neutrons scattered at 90 deg from a sample of liquid para-hydrogen having a nominal thickness of 1 mm. Here, as in all subsequent measurements, the data have been corrected for the background measured with cadmium interposed between the moderator

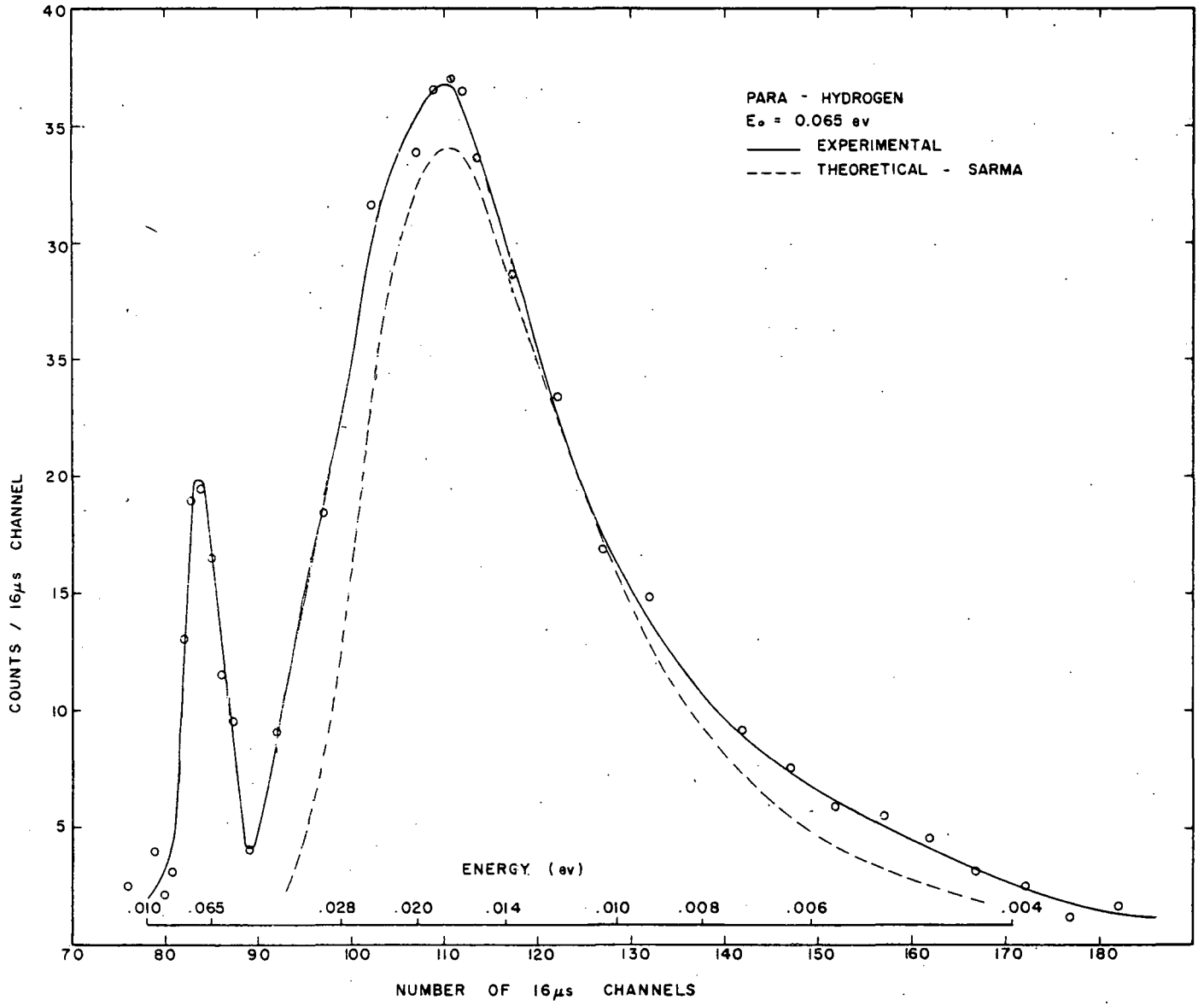

Fig. 19.--The experimental data for neutrons of 0.065 ev scattered by 1-mm layer of para-hydrogen (The theoretical predictions based on a perfect gas model are also shown

neutron source and the chopper. This method of measuring background was adopted because it includes the moderation of the general "fast" neutron background by the sample. It does not, however, account for the elastic scattering from the container which appears as the relatively sharp peak centered at E_o in the data. The dashed curve represents the predicted theoretical scattering corrected for instrument resolution and plotted with an arbitrary normalization. Though the experimental and theoretical curves agree in position the observed broadening, 0.020 ev, is approximately 20 percent greater than the predicted value of 0.017 ev.

Similar representation of the scattering from ortho-para-hydrogen are shown in Figs. 20 and 21 where the incident neutron energies were 0.065 ev and 0.040 ev respectively Comparable measurements have also been made utilizing other incident neutron energies (see Figs. 22, 23, and 24) and in all cases the observed broadening is greater than predicted on the basis of a perfect gas model. Although the theoretical curves were plotted in these figures with arbitrary normalization, it may be useful for future reference to compare the relative theoretical and experimental values for two of these cases (see Figs. 19 and 20). For E_o = 0.065 ev and for the peak of the scattered neutron distributions

$$\left(\frac{d\sigma}{d\Omega dE}\right)_{p\text{-}H} \Big/ \left(\frac{d\sigma}{d\Omega dE}\right)_{o\text{-}p\text{-}H} = 1.93 \text{ and } \sim 3.7 \text{ respectively for the}$$

theoretical and experimental curves.

Since the sample thicknesses were chosen to have a neutron transmission greater than or equal to 0.85, the effects of multiple scattering are believed to be small in most of the cases examined. This assumption has been reinforced by measuring the distribution of neutrons scattered from a sample of para-hydrogen having half the thickness used in obtaining the data in Fig. 19. The observed widths agree within the experimental error. On the basis of these considerations, the observed additional broadening of the distributions appears to be a feature of the liquid state of hydrogen.

3.3 DISCUSSION OF INELASTIC SCATTERING IN LIQUID HYDROGEN

The overall agreement between theory and experiment supports the generally accepted concept that the molecules in liquid hydrogen behave very nearly as they do in a "perfect" gas. The absence of appreciable bonding forces is evident from the agreement between the observed and calculated energies of the various scattering components. Such would not be the case if even moderate binding forces were operative, since the effective mass of the recoiling molecule would then be

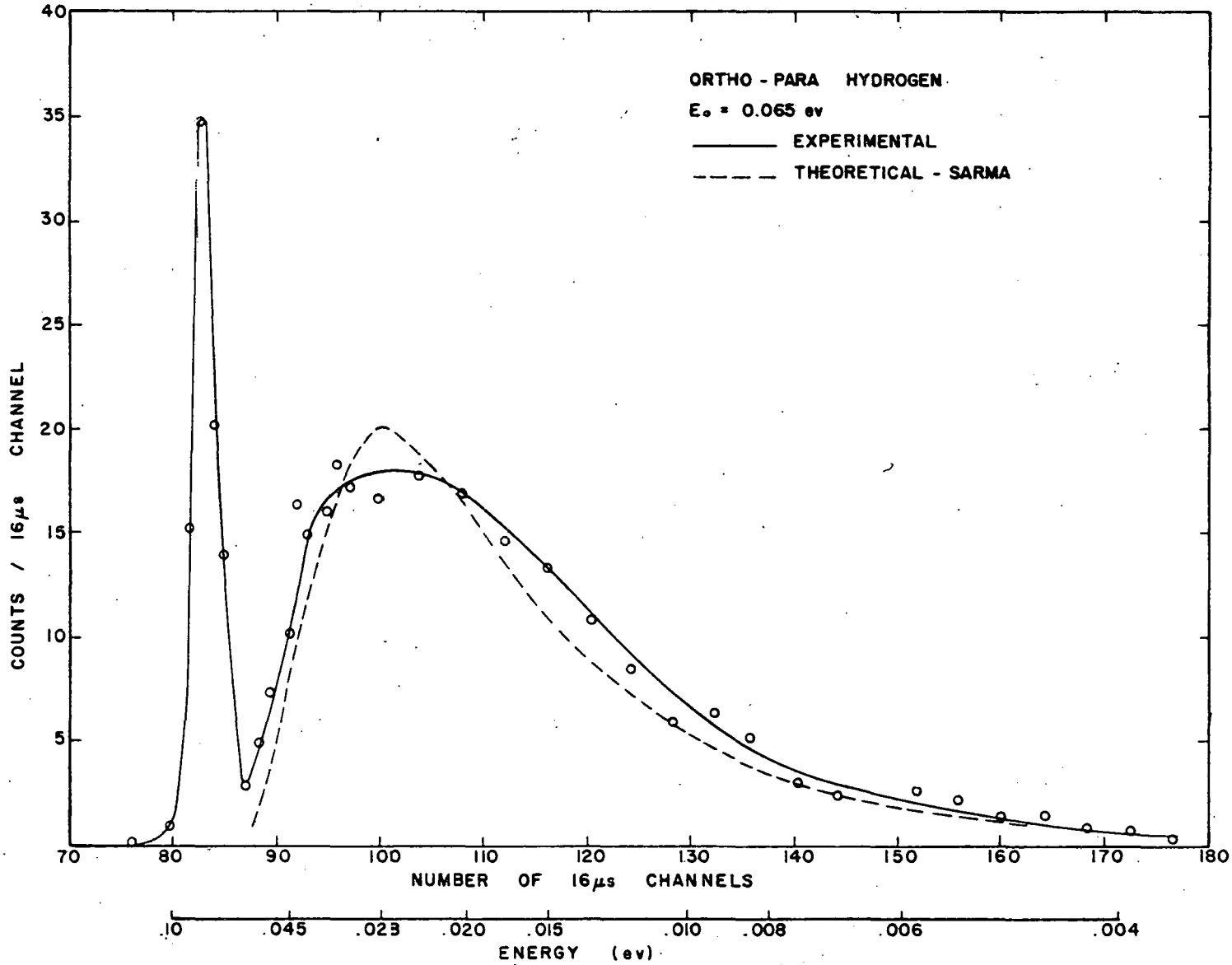

Fig. 20.--The experimental data for neutrons of 0.065 ev scattered by a 1-mm layer of ortho-para-hydrogen (The theoretical predictions based on a perfect gas model are also shown

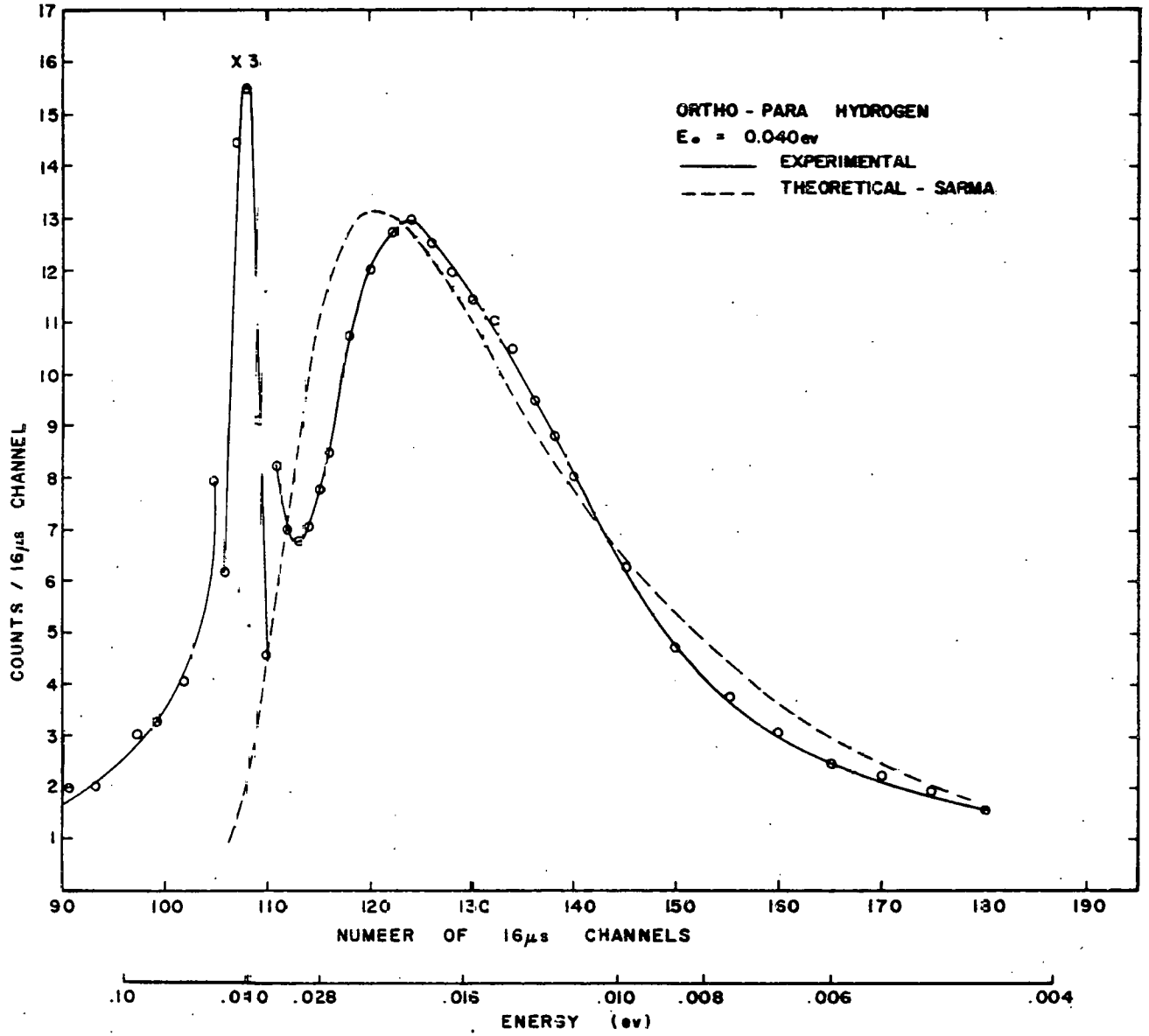

Fig. 21.--The experimental data for neutrons of 0.040 ev scattered by a thin layer of ortho-para-hydrogen (The theoretical predictions based on a perfect gas model are also shown)

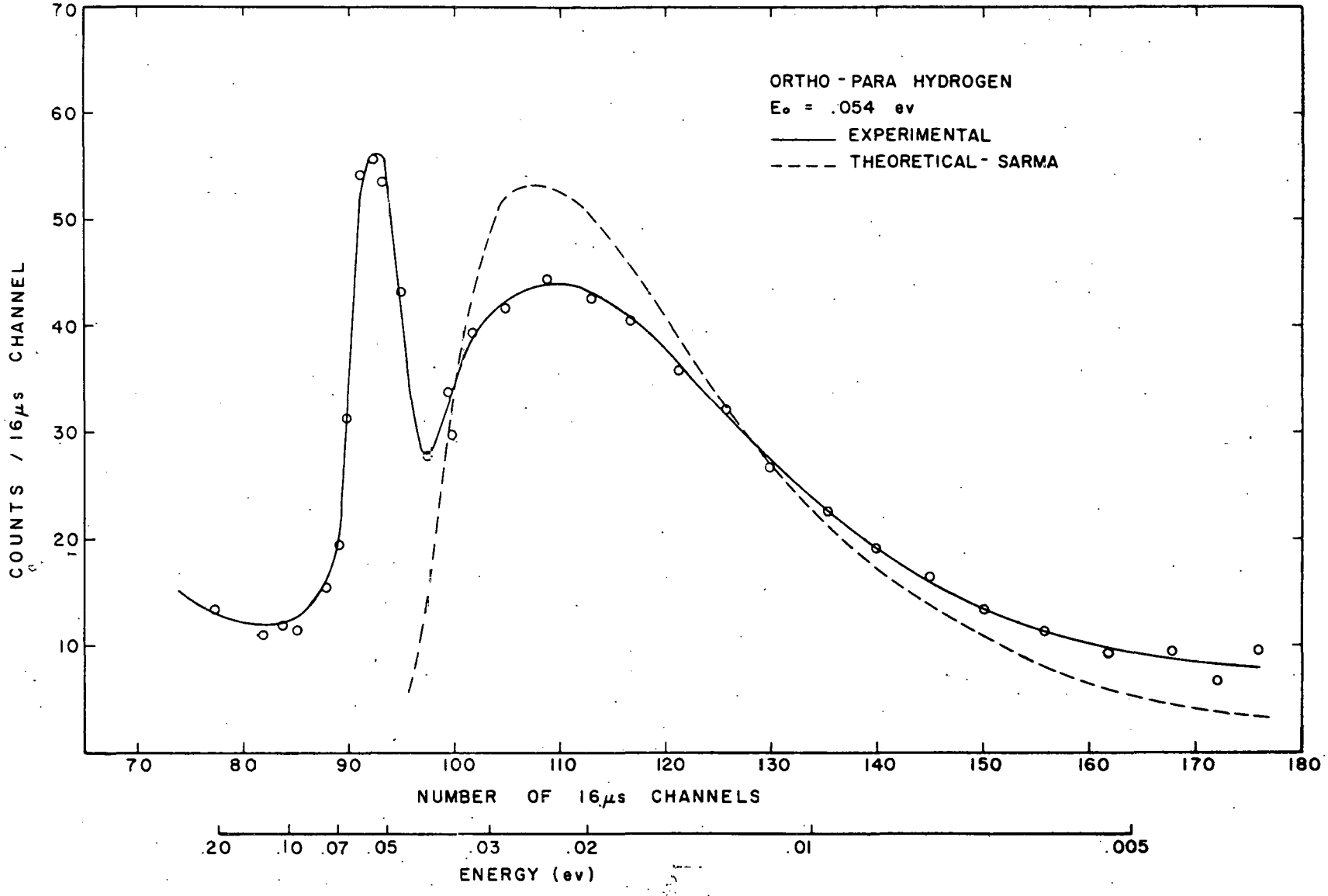

Fig. 22.--The experimental data for neutrons of 0.054 ev scattered by a thin layer of ortho-para-hydrogen (The theoretical curve is based on a perfect gas model)

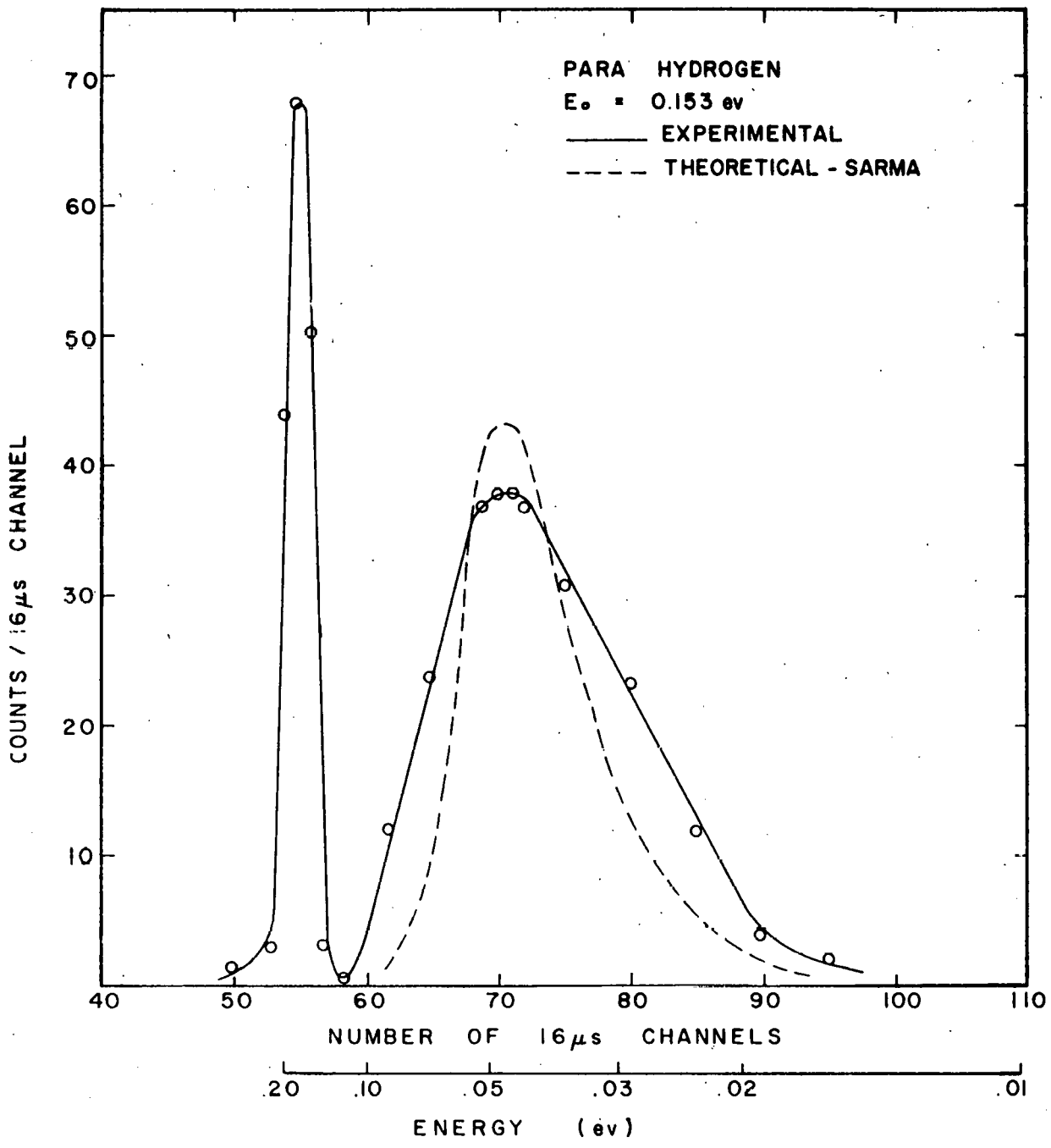

Fig. 23.--The experimental data for neutrons of 0.153 ev scattered by a thin layer of para-hydrogen (The theoretical curve is based on a perfect gas model)

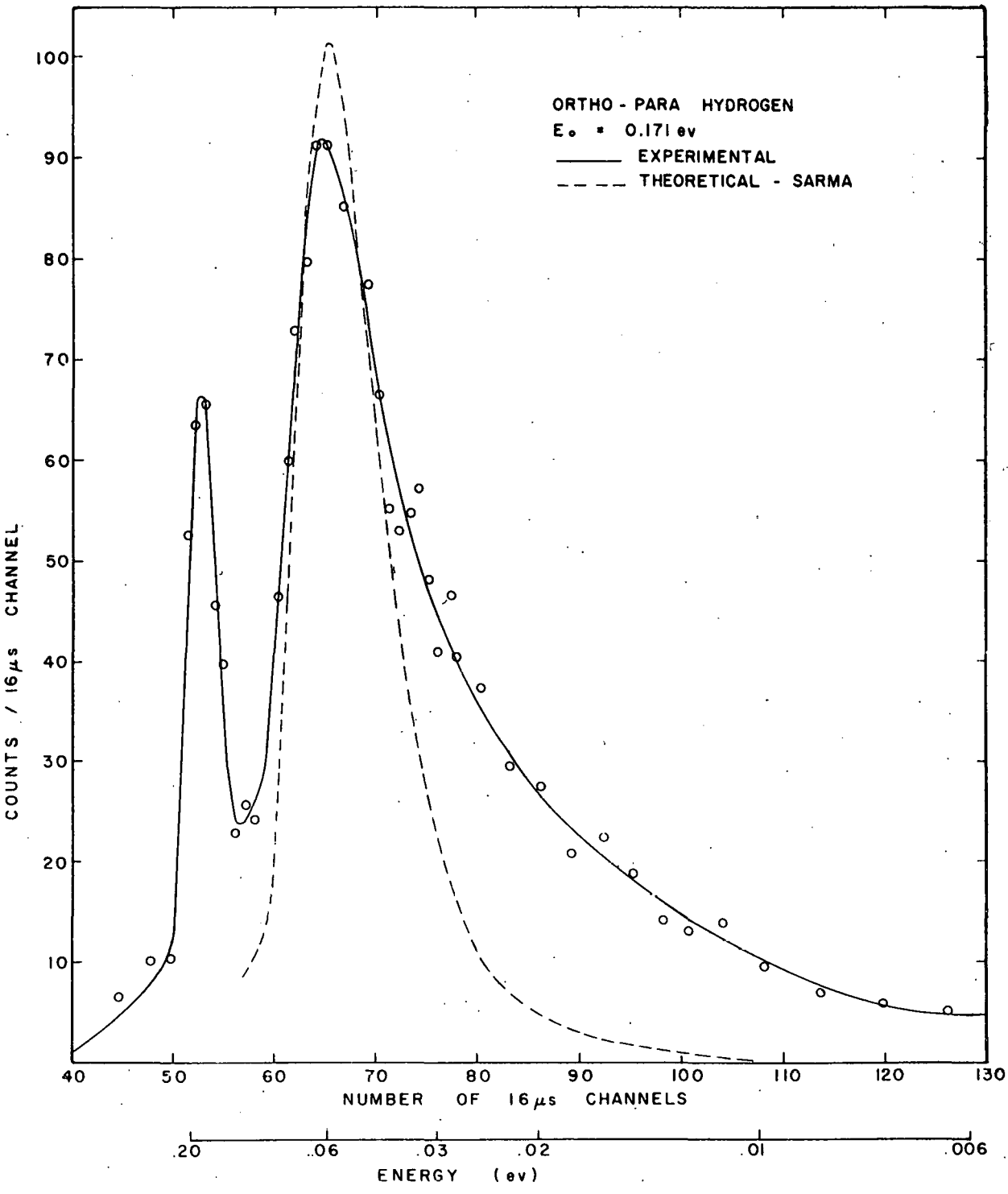

Fig. 24.--The experimental data for neutrons of 0.171 ev scattered by a thin layer of ortho-para-hydrogen (The theoretical curve is based on a perfect gas model)

increased with a substantial reduction in the energy of the recoiling molecule. The position of the peaks of the scattering distributions is thus relatively sensitive to the recoil mass. Moreover, any tendency of liquid hydrogen to exhibit solid state characteristics would be reflected in a reduction of the width of the scattered distribution.

The present data, though not sufficiently accurate to permit final conclusions, indicate that the scattering components are broader than one would expect from the "perfect" gas model. One interpretation of this additional broadening is that the effective translational energy of a hydrogen molecule in the liquid state is larger due to molecular interactions. Theoretical conclusions of Pauling[5] and measurements of Raman spectra[6] support the supposition that the molecules in liquid hydrogen rotate freely. However, the motion of the hydrogen molecules may involve at least two different aspects of the liquid. On the one hand, if there are general nearest-neighbor collisions between molecules, additional broadening of all scattering components should be observed. On the other hand, if the main effect of the liquid state is to reduce the lifetime of the excited states thus introducing a further lack of sharpness in the excited levels, then the $(0 \rightarrow 0)$ scattering distribution in para-hydrogen should not be additionally broadened but all other neutron interactions involving excited states should exhibit extra broadening. Nuclear magnetic resonance measurements[7] of the dependence of the nuclear relaxation time on different concentrations of ortho hydrogen have shown that an interaction exists between ortho and para hydrogen molecules. In view of this interaction, the final state of the neutron scattering event which consists of a single ortho molecule surrounded by para molecules is not well defined and may be an explanation for the extra broadening observed in the present experiment on para-hydrogen. The broadening of the distribution from ortho-para-hydrogen (see Fig.20) appears to be greater than that from para-hydrogen (see Fig.19). Nuclear magnetic resonance measurements[7] have demonstrated clear evidence that the ortho-ortho quadrupole interaction is very strong and much stronger than the ortho-para interaction. This strong ortho-ortho interaction could be the mechanism by which neighboring molecules interact and hence give an extra broadening to the distribution in energy of neutrons scattered by ortho hydrogen. A future experiment on the "elastic" scattering $(0 \rightarrow 0)$ of neutrons in para-hydrogen with $E_o < 0.030$ ev should provide considerable clarification of these effects and may give evidence of an interaction of para molecules with other para molecules, an interaction which cannot be studied directly by the techniques of nuclear magnetic resonance. The experiment has not been performed as yet with the present experimental arrangement due to the very small cross section of the $(0 \rightarrow 0)$ scattering in para-hydrogen.

The positional discrepancy between the experiment and theory shown in Fig. 21 has not been confirmed by repeating the measurements. A crude estimate of multiple scattering indicates only a small effective displacement of the peak to be expected for this scattering (with perhaps the main effect being an enhanced low energy tail). A definitive check on this will be made by observing the scattering from a thinner scattering layer. Assuming the validity of the discrepancy, an explanation is that the liquid state of hydrogen alters the relative cross sections for excitation and de-excitation. If this explanation is correct, the data of Fig. 21 indicates that the $(0 \rightarrow 1)$ transition is enhanced and/or the $(1 \rightarrow 0)$ transition is suppressed in liquid ortho-para-hydrogen. The relative cross sections for scattering by para-hydrogen and ortho-para-hydrogen, noted in the previous section for $E_o = 0.065$ ev, offer additional evidence that the liquid state affects the magnitude of the partial cross sections.

3.4 TOTAL SCATTERING CROSS SECTION IN LIQUID HYDROGEN

Early in this contract year a few additional measurements were made of the total scattering cross section in para-hydrogen in order to check on the influence of the inelastic level $(0 \rightarrow 1)$ on the cross section. Earlier measurements reported last year [1] were made with the small chopper mentioned in Section 2.1.5 to improve the time resolution for measurements in the energy range 0.010 to 0.020 ev. Unfortunately, the low beam intensity of the older linear accelerator limited the statistics of the results. The measurement has been repeated with the present higher power accelerator and the results are shown in the insert in Fig. 25. It is seen that the onset of the excitation of the excited levels is marked. Furthermore, the shape of the main curve for para-hydrogen in Fig. 25 for $E \sim 0.010 - 0.020$ ev is seen to differ from that of the inset and reflects the effect of the poorer time resolution. Except at the energy of the abrupt change of the total cross section, the effect of the poorer resolution on the remainder of the cross section curve is negligible.

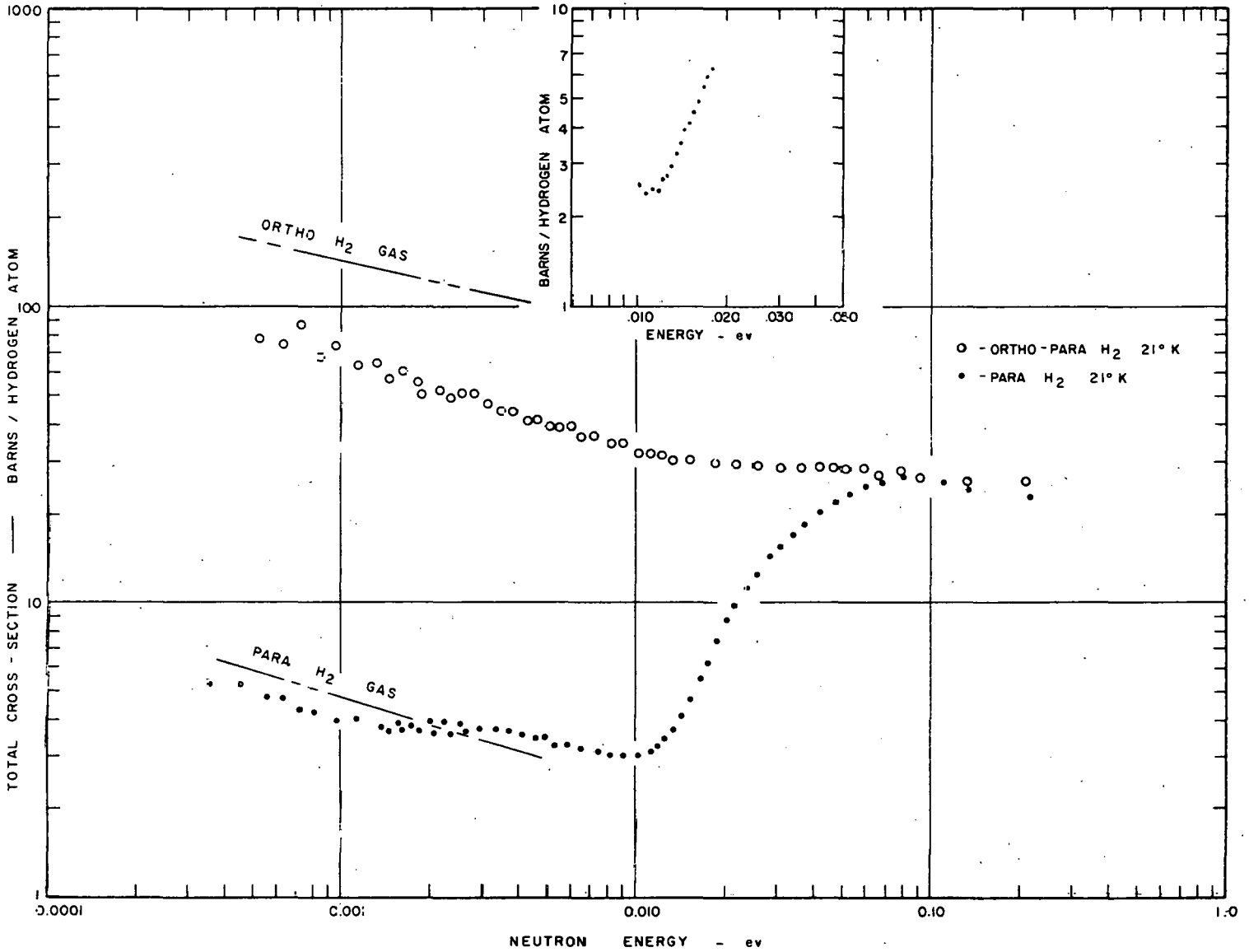

Fig. 25.--The total removal cross section for liquid para hydrogen and liquid ortho-para-hydrogen (Note the cross section for liquid para hydrogen around the sharp discontinuity at ~0.013 ev shown in the insert and obtained with improved energy resolution)

IV. NEUTRON INELASTIC SCATTERING OF POLYETHYLENE

Only preliminary inelastic scattering neutron measurements in polyethylene are available at present. Since additional data are regularly becoming available in this program, this report will outline briefly only the first broad features of the scattering and the preliminary conclusions of a comparison with theory.

4.1 THEORY

A theory of neutron interactions in polyethylene has been developed by D. Goldman[8]. In this treatment, several of the broad features of the Nelkin [9] theory for neutron scattering in water have been appropriately altered to apply to the solid CH_2. In this case, the basic similarity is the molecular component H-C-H compared to H-O-H. The basic differences are that H_2O is a liquid and $(CH_2)_n$ is a solid and further, that the molecular component H-C-H is bound in a long polymerized chain molecule. The similarity between the molecules is reinforced by the values of the rotational and vibrational levels shown in Table 5.

Table 5

COMPARISON OF ENERGY LEVELS IN H_2O AND CH_2

Level	CH_2(ev)	H_2O(ev)
rotation	0.089	~ .06
vibration	.187	.205
vibration	.354	.474
vibration	.533	.488

In Goldman's development of the moderation in polyethylene, he derived a scattering kernel $\sigma(E_o, E, \theta)$. This can be represented as:

$$\sigma(E_o, E, \mu) = \sigma^o(E_o, E) + \mu\sigma^1(E_o, E) + 1/2\,(3\mu^2-1)\sigma^2(E_o, E) + 1/2\,(5\mu^3-3\mu)\sigma^3(E_o, E)$$

when $\mu = \cos\theta$ and the values of σ^1 have been tabulated for an appropriate matrix of suitable energies for E_o and E, ranging from 0.001 ev to 0.625 ev.

4.2 PRELIMINARY EXPERIMENTAL RESULTS

The experimental arrangement shown in Fig. 2 and discussed in detail in Section II was used to study neutrons scattered by polyehtylene. In this preliminary study only neutrons scattered at 90 deg were studied though measurements at other angles will be studied in the future. In Fig. 26, the experimental results for E_o = 0.0092 ev are compared with a calculation based on Goldman's theory for E_o = 0.010 ev, the nearest energy mesh point. An examination of the experimental curve in Fig. 26 shows, for shorter flight times (higher energies), an intensity and time distribution of scattered neutrons that is usually associated with the acoustical modes of a solid. The agreement between the theory and experiment is not very good. In fact, only by removing the "elastic" peak can anything approaching agreement be reached. However, the "elastic" peak must be included for a direct comparison with the theory. Notice that the "elastic" peak is about as narrow as permitted by the resolution of the apparatus, indicating probably that the peak really is very narrow, as one expects if the hydrogen is quite tightly bound to the molecule and has thereby a large effective mass. The absolute cross section has not been determined as yet for the experimental curve. It is also to be noted that previous "cold" neutron measurements[10] on $(CH_2)_n$ were performed with a cold filter and thus could study only energy gain. Palevsky's measurement[10] indicated a broad resonance level in the energy range 0.010 - 0.030 ev. This would be consistent with the present observation. It is gratifying to note that the results obtained last year[11] for polyethylene, using a much simpler arrangement to study inelastic scattering, agree with the present ones.

The representation on a time-of-flight scale, as in Fig. 26, automatically emphasizes the neutron collisions which represent larger energy transfers. When these data are transformed to an energy scale through multiplication by ($t^3 dN/dE = t^3\, dN/dt$) the data at longer flight times (lower energies) are emphasized with respect to those at shorter times. Thus the phonon distribution indicated in the experimental data in Fig. 26 becomes much less outstanding when transformed to an energy distribution as in Fig. 27. Also shown in Fig. 27 is the Goldman theoretical prediction which exhibits quite differently the discrepancy between theory and experiment.

The experimental data in Fig. 28, 29, and 30 for E_o = 0.013, 0.020, and 0.040 ev also show evidence for solid state effects in the broadened wings of the distributions, both for energy-loss, as well as energy-gain scattering. Because of the somewhat poorer instrumental resolution for these measurements, it is not entirely clear whether the "elastic" peak from $(CH_2)_n$ is broadened by the instrumental resolution as was the case for

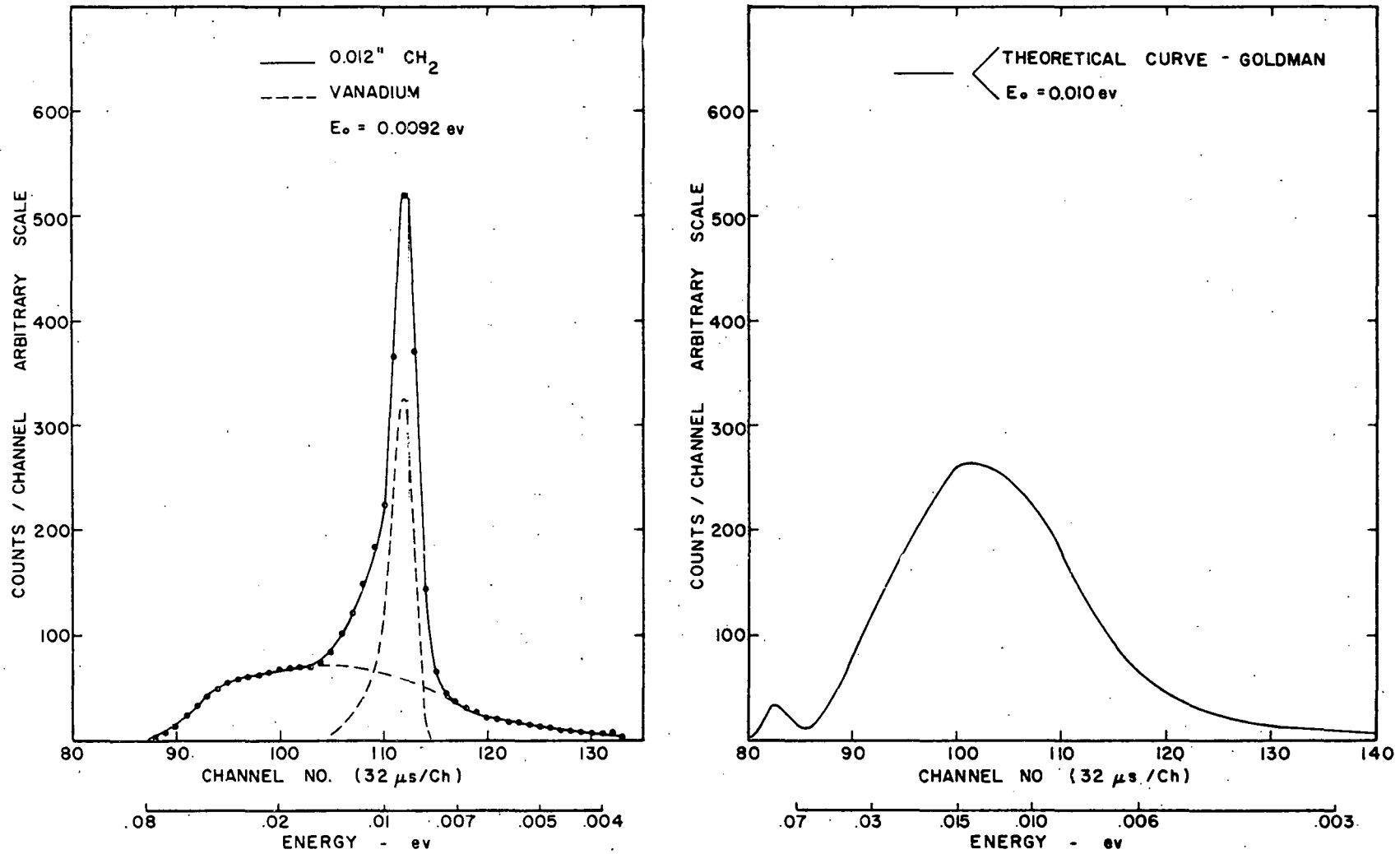

Fig. 26.--The inelastic scattering of neutrons at φ = 90 deg with E_o = 0.0092 ev for a thin layer of polyethylene (Also shown is the time resolution obtained by scattering from vanadium and the theoretical prediction based on Goldman' s kernel)

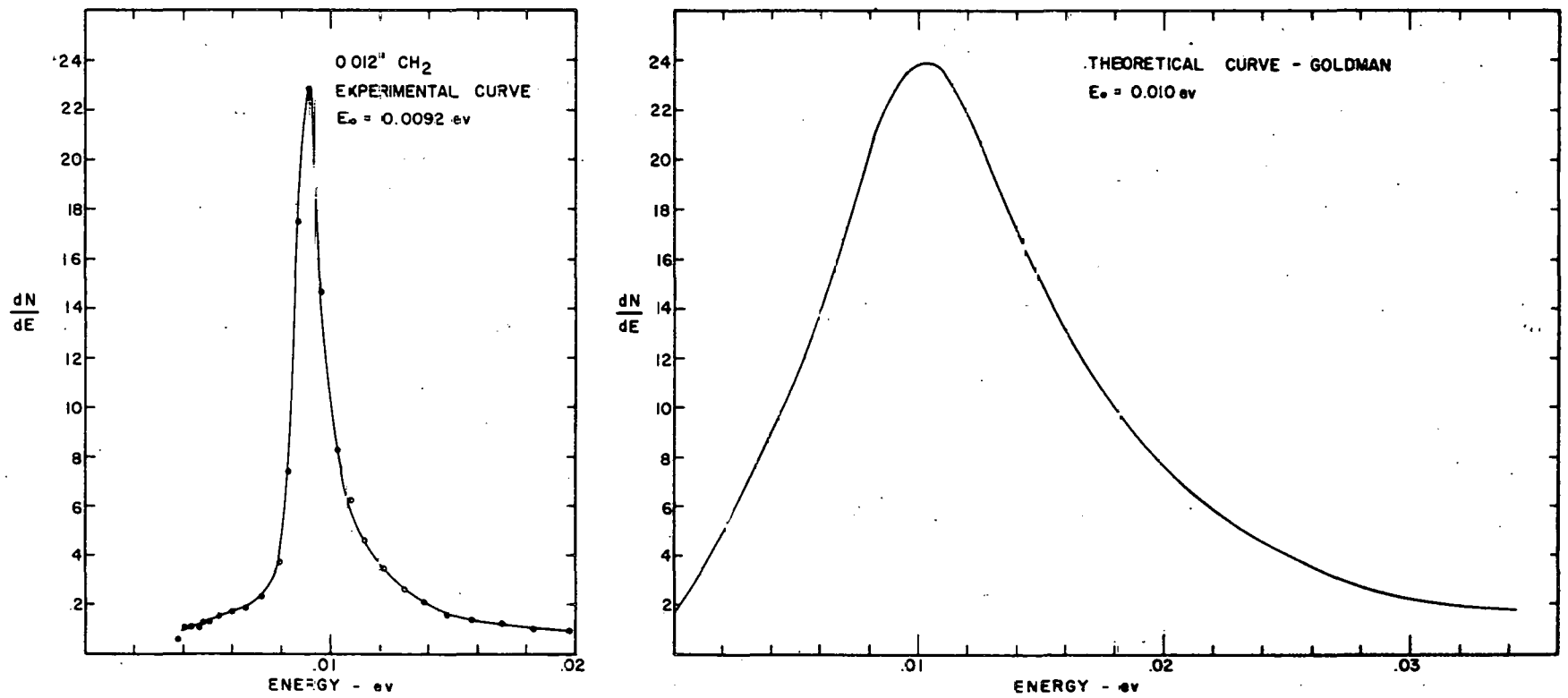

Fig. 27.--An experimental energy distribution of neutrons of 0.092 ev scattered at 90 deg by a thin layer of polyethylene (A theoretical distribution for E_o=0.010 ev based on Goldman's kernel is also shown)

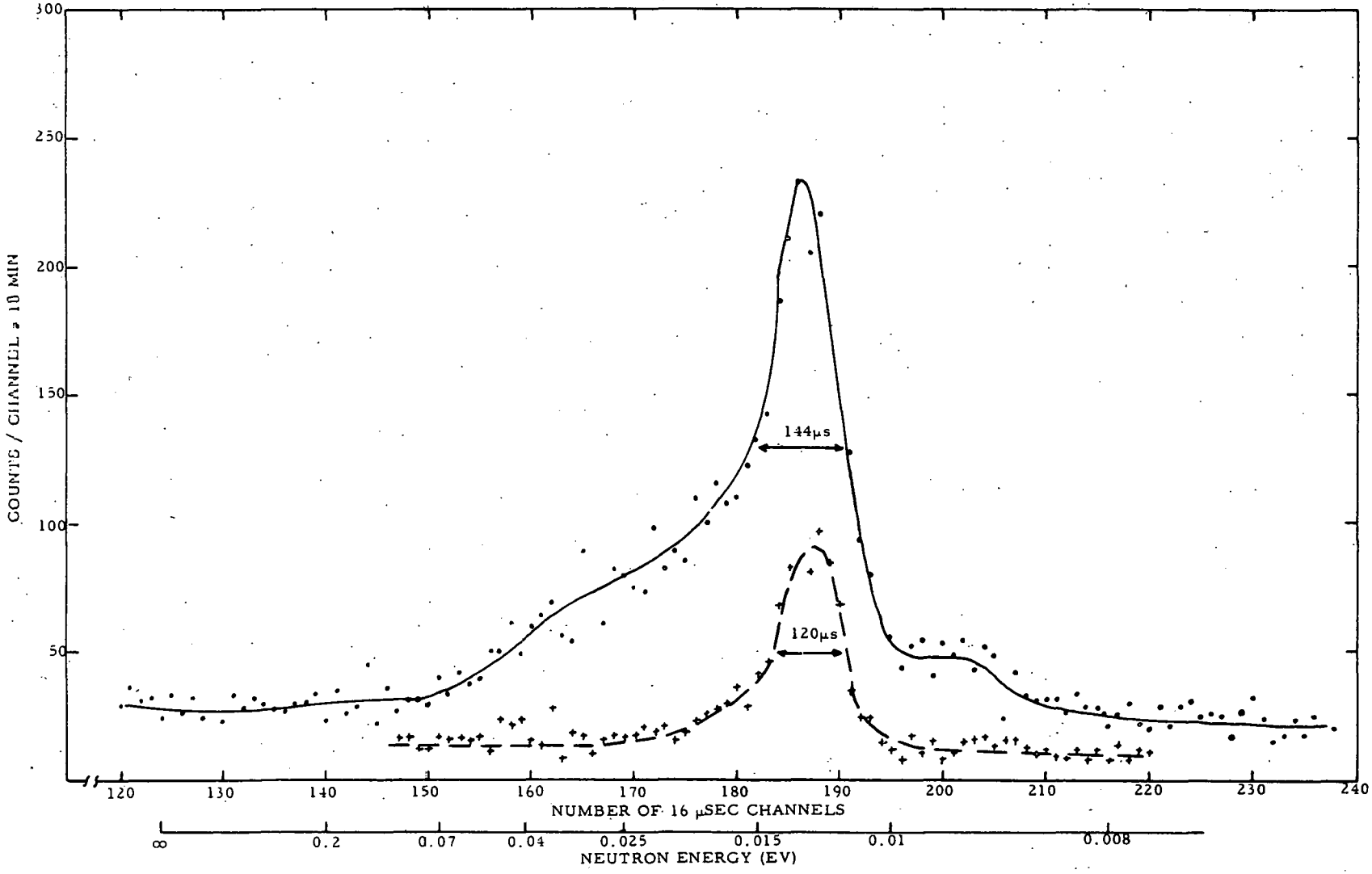

Fig. 28.--The time-of-flight distribution of neutrons with E_o=0.013 ev scattered by a thin layer of polyethylene (The incident beam resolution is shown by the scattering from vanadium)

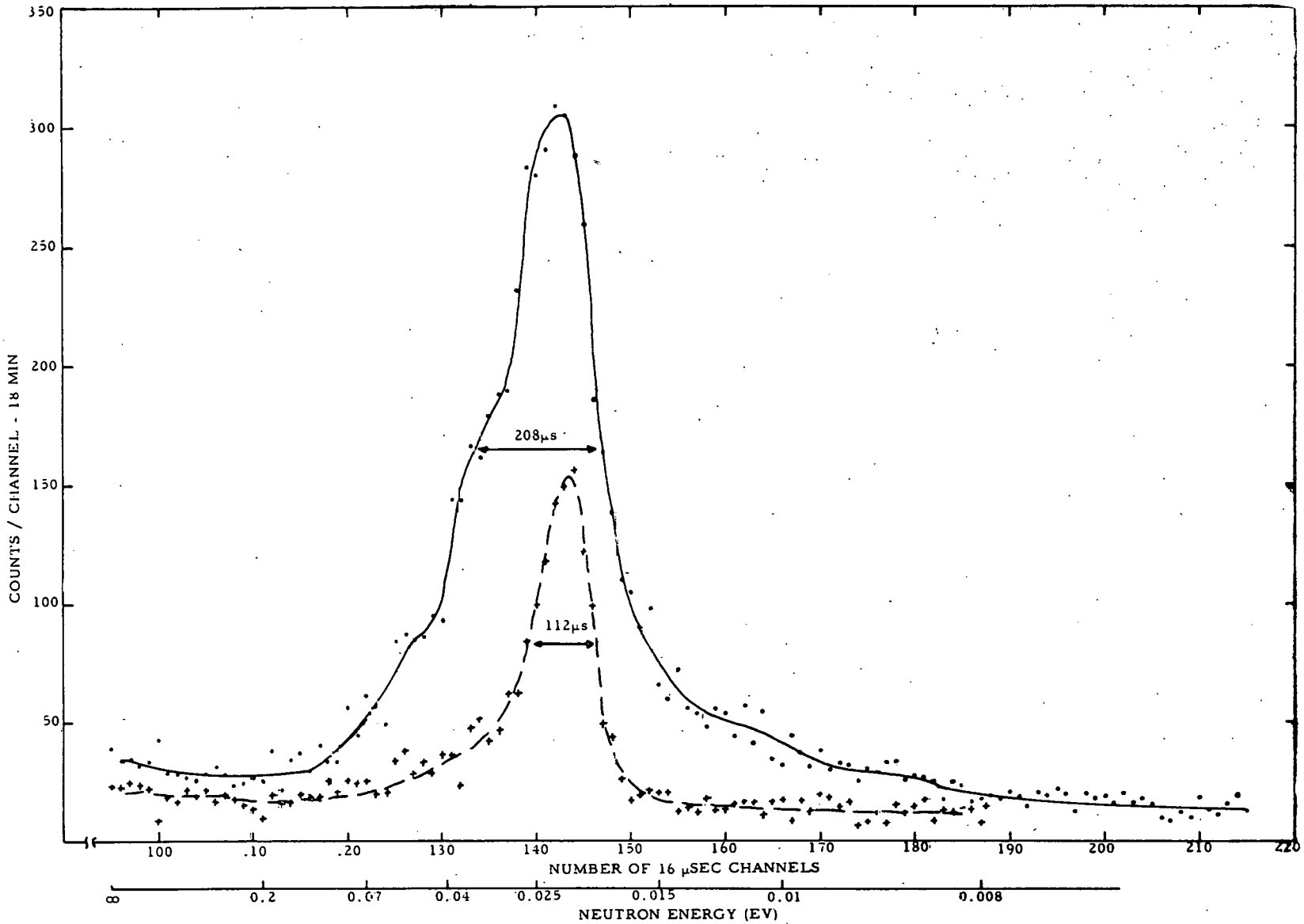

Fig. 29.--The time-of-flight distribution of neutrons with E_o=0.022 ev scattered by 90 deg by a thin layer of polyethylene (The incident beam resolution is shown by the scattering from vanadium)

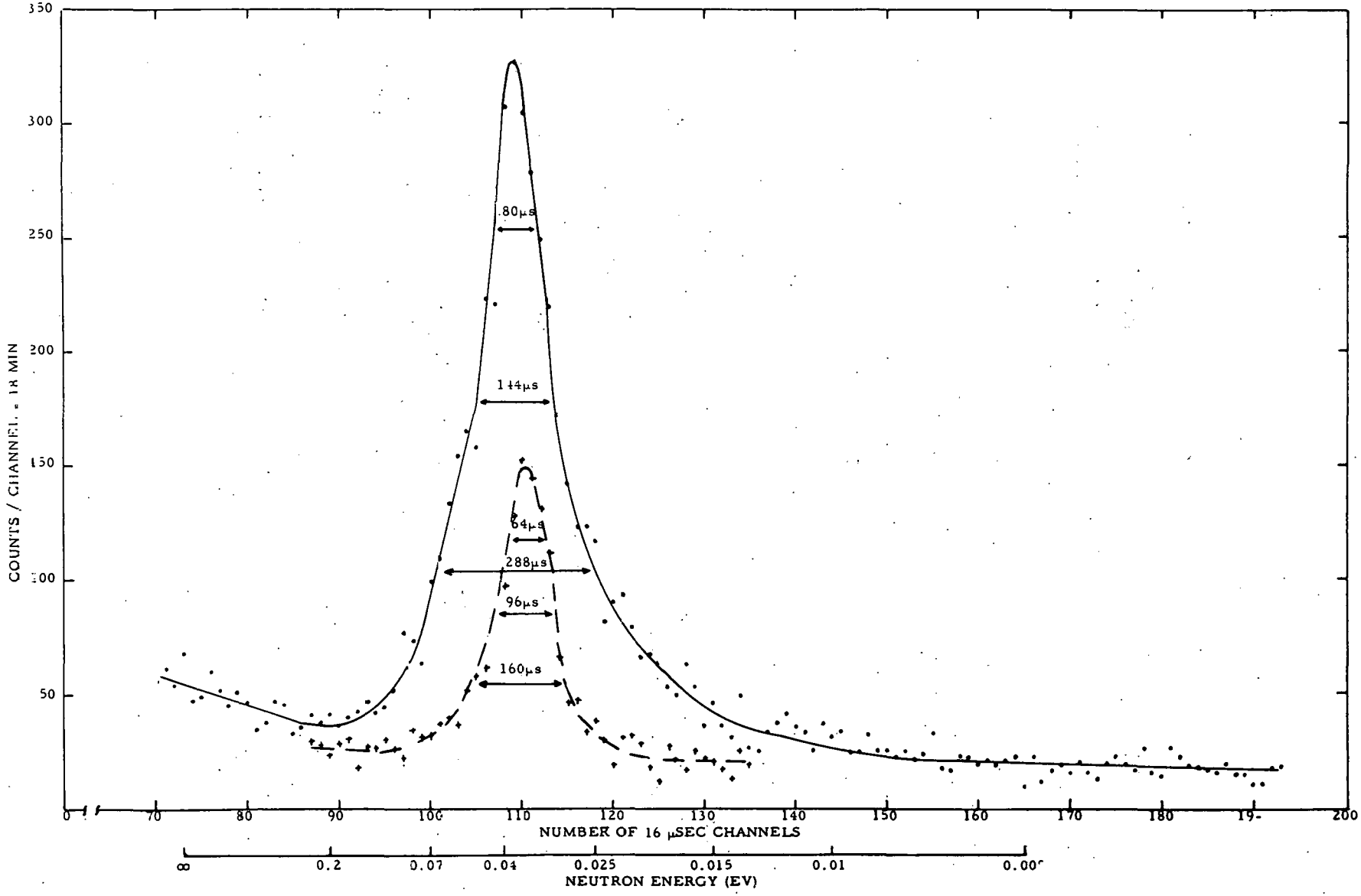

Fig. 30.--The time-of-flight distribution of neutrons with E_o=0.038 ev scattered at 90 deg by a thin layer of polyethylene (The incident beam resolution is shown by the scattering from vanadium)

lower incident energy, or whether there is an inherent broadening of the "elastic" peak in $(CH_2)_n$. It appears, however, that there is some inherent broadening of the level. A summary of the theoretical predictions calculated from Goldman's theory is shown in Fig. 31 for pertinent values of incident neutron energies ranging from 0.006 ev to 0.100 ev plotted on a time-of-flight scale for ready comparison with the experimental data. The discrepancy between theory and experiment just discussed in some detail for the case of E_o = 0.0092 ev, is repeated for the higher incident energies shown in Figs. 28, 29 and 30 but is not so pronounced. Since it is generally acknowledged that solid state effects are best studied for "cold" neutrons ($E \lesssim 0.005$ ev), it is not surprising that such effects appear in the present results most clearly for E_o = 0.0092 ev and less clearly for $0.013 < E_o < 0.040$ ev.

The latest experimental result for $(CH_2)_n$ is shown in Fig. 32 for E_o = 0.089 ev. For this experiment, better energy resolution, occasioned in part by a higher rotational speed for the chopper (180 rps), was available as indicated by the narrow time distribution of neutrons scattered by vanadium. It is clear for this case that the "elastic" peak has an inherent broadening and, in addition, a substantial low-energy tail which corresponds to the known moderating power of $(CH_2)_n$. Goldman's kernel predicts a distribution with an approximately correct shape but which is narrower than observed. It is to be noted that no corrections were made for multiple scattering. However, since the specimen is "thin" with a transmission larger than 0.85 in all cases, these corrections are believed to be small and the disagreement is believed to be real.

A detailed examination of the above results is underway but the results are not yet available. To summarize the preliminary discussion above for $(CH_2)_n$, and placing somewhat more reliance on the results for E_o = 0.0092 and 0.089 ev, the scattering kernel of Goldman predicts that:

1. For the very low incident energies (<0.040 ev) the distribution is too broad and has the wrong shape, due most likely in the main to an omission in the theory of the solid state acoustical modes.

2. For the higher incident energies (~0.100 ev), the shape of the scattered neutron energy distribution is approximately correct although the predicted width is narrower than observed.

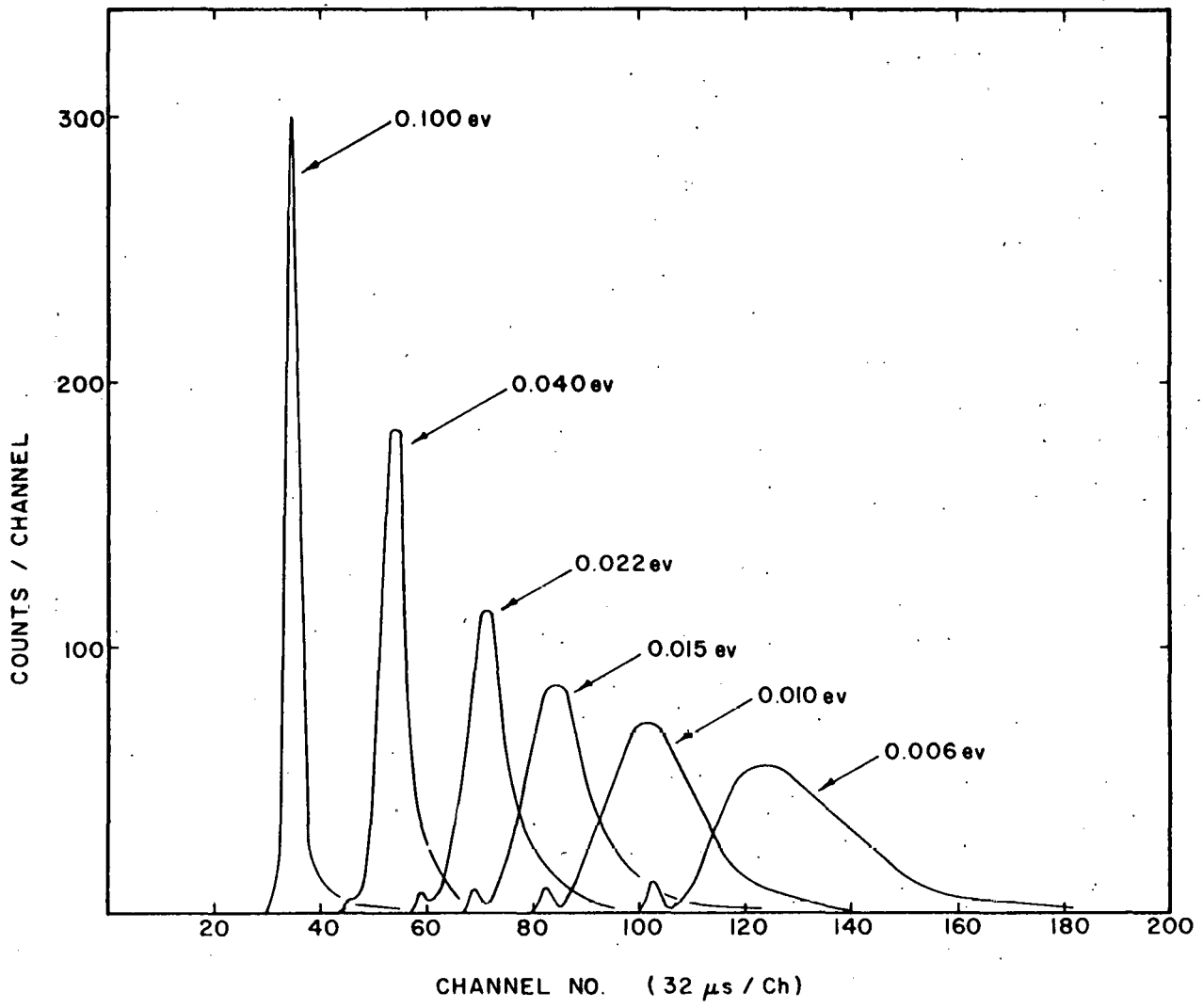

Fig. 31.--Theoretical predictions of the scattering at 90 deg from polyethylene for a number of different incident energies (The data are exhibited on a time-of-flight scale to facilitate comparison with the experimental data)

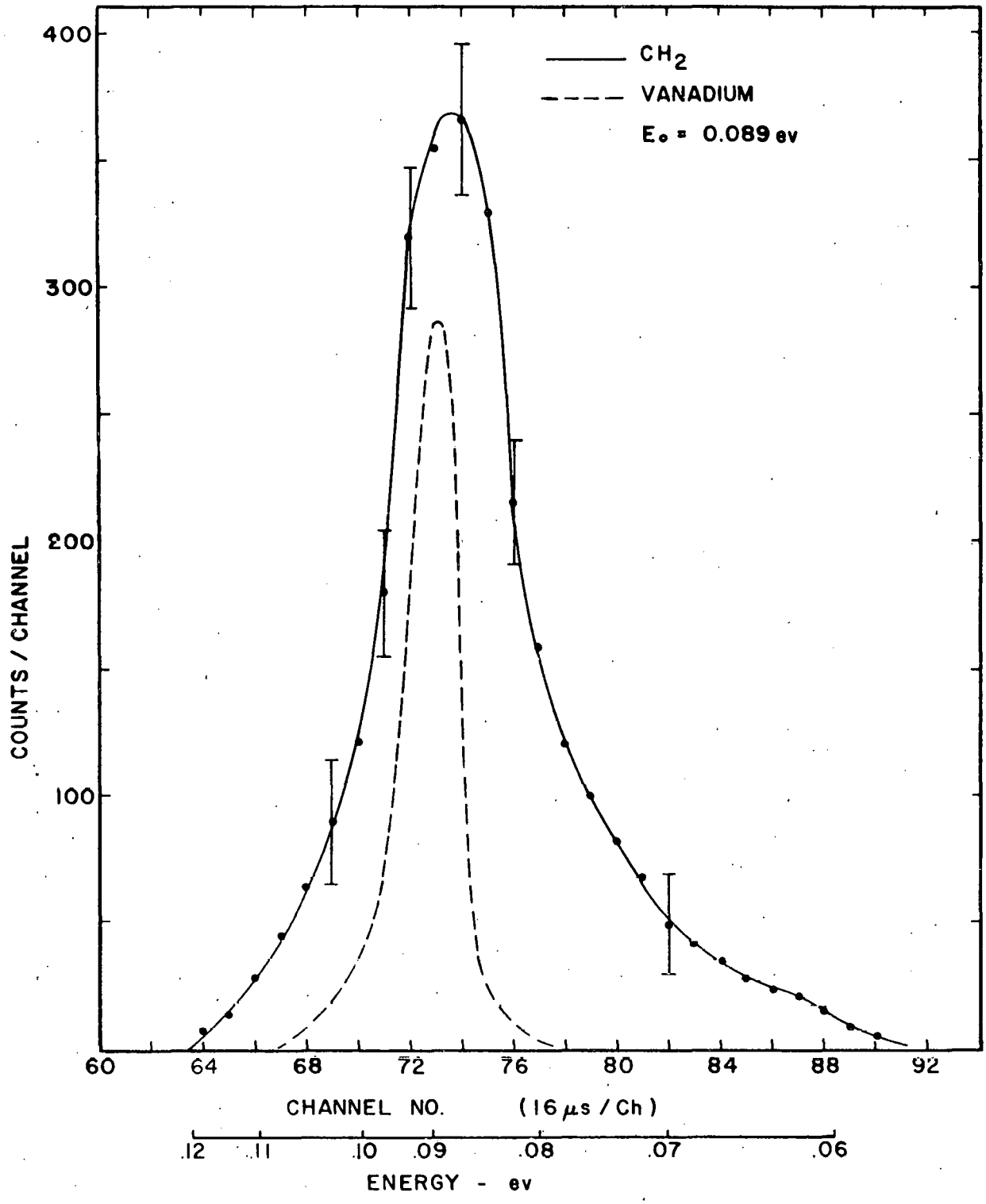

Fig. 32.--The time-of-flight distribution of neutrons scattered from a thin layer of polyethylene at φ = 90 deg with E_o = 0.089 ev (the resolution of the incident beam is shown by the scattering from vanadium)

REFERENCES

1. W. L. Whittemore and A. W. McReynolds, General Atomic Report GA-2503 dated October 30, 1960. Annual Summary Report for Contract AT(04-3)-167 "Differential Neutron Thermalization," for the period of October 1, 1960 through September 30, 1961.

2. M. F. Crouch, Nucl. Sci. and Eng. 2, 631 (1957).

3. G. Sarma, "Inelastic Scattering of Neutrons in Solids and Liquids" (IAEA, Vienna, 1961) p. 397.

4. L. Van Hove, Phys. Rev. 95, 249 (1954).

5. L. Pauling, Phys. Rev. 36, 430 (1930).

6. J. C. McLennon and J. H. McLeod, Nature 123, 160 (1929).

7. A. Abragam, "The Principles of Nuclear Magnetism," Oxford Univ. Press, 1961, p. 223 ff.

   Hass, Seidel, and Poulis, Physica, Deel 26, 834 (1960). Both of these include extensive additional references to pertinent literature.

8. D. Goldman, Knolls Atomic Power Laboratory, private communication.

9. M. Nelkin, Phys. Rev. 119, 741 (1960).

10. Myers, Cotter, and Palevsky, Phys. Rev. Abstra. II, Vol. 6 (April 1961) paper L.8.

11. Reference 1, page 65 ff.